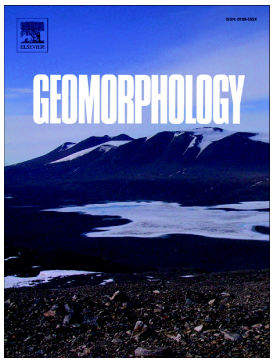

Evidence of Quaternary tectonics along Río Grande valley, southern Malargüe fold and thrust belt, Mendoza, Argentina

Bruno Colavitto, Lucía Sagripanti, Lucas Fennell, Andrés Folguera, Carlos Costa

PII: S0169-555X(19)30278-8
DOI: https://doi.org/10.1016/j.geomorph.2019.06.025
Reference: GEOMOR 6812

To appear in: *Geomorphology*

Received date: 4 September 2018
Revised date: 15 June 2019
Accepted date: 29 June 2019

Please cite this article as: B. Colavitto, L. Sagripanti, L. Fennell, et al., Evidence of Quaternary tectonics along Río Grande valley, southern Malargüe fold and thrust belt, Mendoza, Argentina, Geomorphology, https://doi.org/10.1016/j.geomorph.2019.06.025

Evidence of Quaternary tectonics along Río Grande valley, southern Malargüe fold and thrust belt, Mendoza, Argentina

Bruno COLAVITTO[1*], Lucía SAGRIPANTI[1], Lucas FENNELL[1], Andrés FOLGUERA[1], Carlos COSTA[2]

[1] *Universidad de Buenos Aires. Consejo Nacional de Investigaciones Científicas y Técnicas. Instituto de Estudios Andinos Don Pablo Groeber (IDEAN). Facultad de Ciencias Exactas y Naturales, Intendente Güiraldes 2160, Ciudad Universitaria, Pabellón II, CP1428EGA, Buenos Aires, Argentina*

[2] *Universidad Nacional de San Luis. Departamento de Geología. San Luis, Argentina*

**Corresponding author (e-mail: bcolavitto@gl.fcen.uba.ar)*

Abstract

The Malargüe fold and thrust belt is developed in the Argentinian Andes between 34º and 37º S, through the tectonic inversion of Upper Triassic and Lower Jurassic depocenters of the Neuquén Basin, with an uplift history since the Cretaceous. Evidence of Quaternary deformation has been described in the northern part of it (34-34.5°S), potentially coeval to neotectonic activity along the eastern edge of San Rafael block. To the south, compressional and extensional structures active during the Quaternary were found in the Dorso de los Chihuidos along the Agrio fold and thrust belt front (37.5-38°S). Contrastingly, the southern segment of the Malargüe fold and thrust belt between these two areas with described neotectonic activity is partially covered by Quaternary products of the Payún Matrú volcanic field, that may hide evidence of recent deformation. In this 300 km gap of neotectonic information, the landscape imprint of two individual structures aligned in the mountain front through the Río Grande valley was analyzed. New evidence of neotectonic deformation were recognized, in particular over the western slope of the Cara Cura range, expressed by faulting and folding of Quaternary deposits and

lava flows. An $^{40}Ar/^{39}Ar$ age from a deformed lava flow at the flanks of an anticline in the foothills of the Cara Cura range may suggest at least an upper Pleistocene compressional tectonic activity. Longitudinal river profile analysis revealed anomalies that show some correlation with the neotectonic structures described, especially knickpoints and concavity index changes. Meanwhile normalized steepness index values showed a moderate response to recent deformation. A proposed schematic geomorphic evolution for this segment of Río Grande river is discussed to put the neotectonic activity into the context of landscape formation. All together this evidence supports the idea of an active front through the Río Grande valley during the Quaternary, coetaneous to an active broken foreland to the east in the southern Central Andes.

Keywords: morphometry; neotectonics; Southern Andes; Payenia

1. Introduction

The present tectonic setting in southern South America is the result of a combination of processes such as the obliquity of subduction, the angle of the subducted slab, the absolute motion of the upper plate and the presence of asthenospheric processes interacting with inherited crustal anisotropies of major or minor hierarchy, among other factors (see Costa et al., 2006a; Folguera et al., 2015 for reviews). Particularly, the Chilean-Pampean Flat Subduction Zone (27-33°S) (Fig. 1a) in the Southern Central Andes constitutes a first order feature and is the main focus of paleoseismic, neotectonic and morphotectonic studies in Argentina (Ramos, 2000; Costa et al., 2000, 2006a). South of 33ºS, in the transition zone from shallow to normal subduction, present and historical seismic records are scarce (e.g. Bohm et al., 2002; Lupari et al., 2015, 2016), although several works have documented neotectonic deformations in cordilleran and extra-cordilleran areas. These works leave, however, a regional gap of information in the southernmost Central Andes, more precisely between the neotectonic structures concentrated among Diamante and Atuel rivers (Bastías et al., 1993; Costa et al., 2006b; Baker et al., 2009; Branellec et al., 2016a) and those located southwards between the Agrio and the Guañacos fold and thrust belts (FTB) (Folguera et al., 2004; Messager et al., 2010, 2014; Huyghe et al., 2015; Sagripanti et al., 2015) (Fig. 1). No neotectonic information is described there, being relevant to provide a complete data coverage along the Andean neotectonic front in order to determine whether Quaternary deformation is absent in that segment or may be obscured in part due to the broad extension of Quaternary volcanism in southern Mendoza province (Fig. 1).

Thus, we focus on this regional gap of data (36º30'S-36º50'S, 69ºW-70ºW), particularly at the Cara Cura and Chihuidos structures that compose the southern Malargüe FTB front (Fig. 1). In this latitudinal segment, evidence of Late Cretaceous and Miocene contractional phases were reported, being possible to delimit two separate domains: one, to the west, along the Malargüe and Agrio FTB fronts (Kozlowski et al., 1993; Cobbold and Rossello, 2003; Ramos and Folguera, 2005; Alvarez et al.,

2013; Fennell et al., 2017) and another towards the east in the San Rafael block and Chical-có plains (Ramos and Kay, 2006; Zárate and Folguera, 2014) (Fig. 1).

Considering that the eastern domain concentrates Quaternary tectonic activity, we aim to identify neotectonic deformations in the western domain. Hence, in this work we present direct field evidence of Quaternary deformation, discuss this evidence in the regional context and analyze their conditioning effect in the geomorphic evolution of this segment of the Río Grande valley. As a first approach to analyze geomorphological evolution, we also performed basic morphometric analysis of drainage networks in Cara Cura and Chihuidos ranges.

As a general agreement, "neotectonics" is a time-dependent definition that may vary according to the geological history of each region (van Hinsbergen, 2010). In the present work, we use the terms "neotectonics", "Quaternary tectonics" or "Quaternary deformation" as synonyms. If expanding the time window to late Pliocene times is required, we will mention this time-lapse explicitly. As stated by Costa et al. (2006a) the terms "neotectonics" or "Quaternary tectonics" include features or structures related to changes in earth surface that may be the consequence of the active or modern stress field and that may provoke an earthquake in the future. Analysis of seismic capability exceeds the purpose of this work, being necessary more exhaustive geomorphological and paleoseismological studies in order to characterize the geometry and seismic potential of the faults and other structures here described.

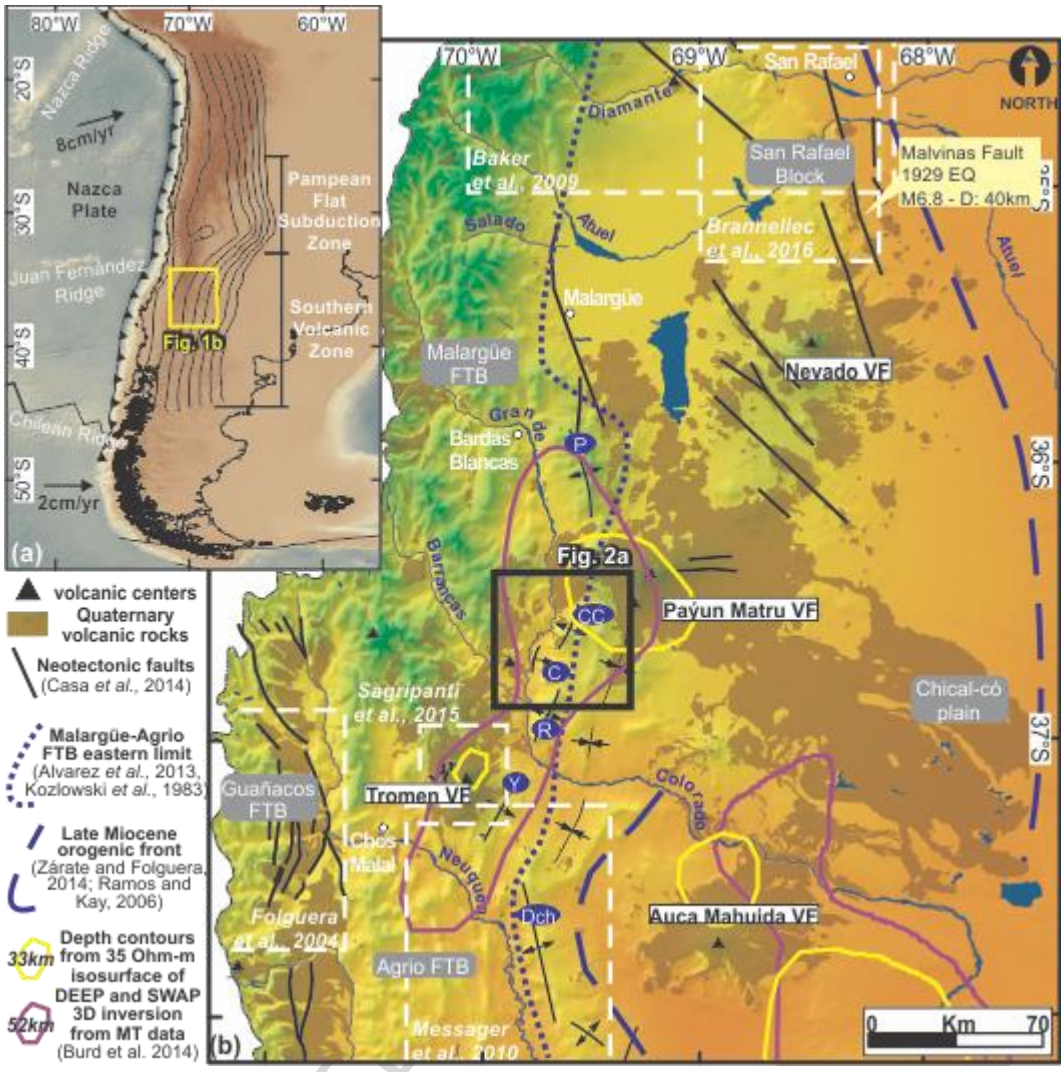

Figure 1. *(a) Regional context of the Southern Central Andes and the location of Figure 1b; Chilean-Pampean Flat Subduction Zone and Southern Volcanic Zone are shown as well as subducted slab depth contours (Tassara and Echaurren, 2012). (b) Main morphostructural units in the study area in the southernmost Central Andes. Structures of interest are labeled in blue ellipses (P: Palauco; CC: Cara Cura; C: Chihuidos; R: Reyes; Y: Yesera; DCh: Dorso de los Chihuidos). White dashed rectangles show recent neotectonic studies in the region (references in white letters). Yellow and violet curves are, respectively, the 33 km and 55 km depth contours of the obtained 35 Ohm-m resistivity from a 3D inversion of a magnetotelluric survey depict an asthenospheric anomaly interpreted as a mantle plume at depth (Burd et al., 2014).*

2. Setting

2.1 Regional setting

The southern Malargüe FTB orogenic front is developed between 36º 30' and 36º 50'S, corresponding to a segment where no neotectonic deformations had been previously identified (Fig. 1). This region corresponds to a thin and thick-skinned deformational belt (Kozlowski et al., 1993; Manceda and Figueroa, 1995; Ramos et al., 2014) that deforms the northern Neuquén basin through the inversion of Late Triassic/Early Jurassic half-graben depocenters (Legarreta and Gulisano, 1989; Branellec et al., 2016b; Cristallini et al., 2009; Giambiagi et al., 2009). This inversion was the result of the opening of southern Atlantic Ocean during middle to Late Cretaceous times and the consequent acceleration of the continent towards the trench, which produced the contractional deformation of Jurassic to Early Cretaceous units (Cobbold and Rossello, 2003; Tunik et al., 2010; Orts et al., 2012; Mescua et al., 2013; Fennell et al., 2017). After this stage, continental foreland basin conditions were established, documented through the largely extended Upper Cretaceous continental red deposits of the Neuquén Group. Then, a period of extensional deformation occurred during the late Oligocene-earliest Miocene associated with increasing retroarc volcanic activity and the formation of extensional depocenters in intra-arc (e.g. Cura Mallín basin; Jordan et al. 2001) and retro-arc positions (e.g. Palauco basin; Silvestro and Atencio, 2009; Álvarez et al., 2013). During middle to late Miocene, constructional mountain conditions were reestablished in the Andes at these latitudes (Giambiagi et al., 2008; Silvestro et al., 2005; Turienzo et al., 2012; among others). This stage is associated with an arc expansion cycle that occurred between ~15 and 5 Ma which involved progression of the deformation towards the east (Kay et al., 2006; Ramos and Kay, 2006; Ramos et al., 2014). This provoked the uplift of San Rafael block and Chical-có plain in the foreland zone (Spagnuolo et al., 2012; Zárate and Folguera, 2014) and synorogenic sedimentation in the Río Grande and Pampa del Carrizalito foreland basins (Silvestro and Atencio, 2009; Sagripanti et al., 2011) (Figs. 1, 2a).

After this period, a steepening of the subducted slab is postulated based on the development of Payenia volcanic province, a large volcanic plateau (ca. 40000 km^2) located as far as 500 km from the present oceanic trench and formed by basaltic lavas, pyroclastic flows, rhyolite domes and cinder cones (Polanski, 1954; Ramos and Folguera, 2011). Recent proposals associate this widespread intraplate volcanism with the presence of two conductive anomalies called DEEP (DEep Eastern Plume) and SWAP (Shallow Western Asthenospheric Anomaly) interpreted as a mantle plume impacting the lower crust (Burd et al., 2014) (Fig. 1b). This major volcanic province groups several volcanic fields (VF) of polygenetic and monogenetic origin with ages that range from the late Pliocene (e.g. Nevado VF) to the Holocene, as recent as 2±2 ka in the Payún Matrú VF (Fig. 1; Dyhr et al., 2013; Marchetti et al., 2014). Locally, in Los Volcanes region, east of the Payún Matrú VF, 25-45 ka -old lava flows have poured and temporarily dammed the Río Grande valley during late Pleistocene times (Fig. 2a; Marchetti et al., 2006; Germa et al., 2010).

Overall, the Quaternary orogenic front to the north of the studied area may be located in the eastern edge of northern San Rafael block, characterized by Las Malvinas Fault System, a reverse fault system which has been associated with the 1929 Mw ~6.0 Las Malvinas earthquake epicenter (Cisneros et al., 1989; Cisneros and Bastías, 1993; Costa et al., 2006b) (Fig. 1). Progressively to the south, Quaternary deformation retreats to the west: the southernmost San Rafael block shows no descriptions of Quaternary reactivations meanwhile, further south, neotectonic activity is located along the eastern limit of Agrio FTB (Dorso de los Chihuidos) and Tromen volcano (Fig. 1). In those regions morphological and structural analyses proved the existence of Plio-Quaternary shortening and uplift (e.g. Galland et al., 2007; Sagripanti et al., 2015, 2016); with limited extensional (Messager et al., 2010, 2014) and strike-slip deformations (Backé et al., 2006).

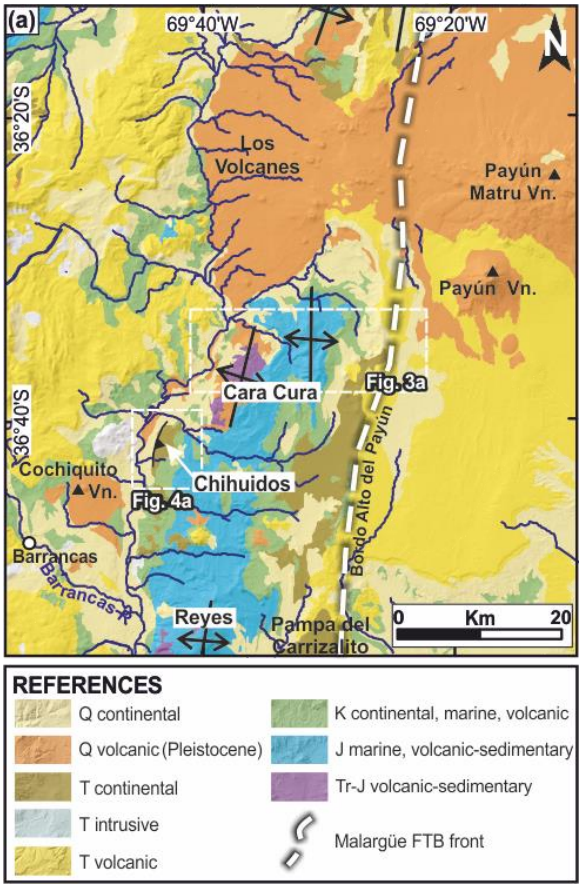

Figure 2. *(a) Geologic map of southern Malargüe fold and thrust belt front (modified from Narciso et al., 2004; Nullo et al., 2005). Q: Quaternary; T: Tertiary; K: Cretaceous; J: Jurassic; P-Tr: Permo-Triassic. Location shown in Figure 1.*

2.2 Local settings

2.2.1 Cara Cura range

The Cara Cura range presents an 800 m relief and is an asymmetric uplifted block cored by Triassic and Jurassic rocks (Fig. 3). It is composed by two major west-vergent anticlines with a slightly different orientation each: a western (NNE-SSO trend) and an eastern one (N-S trend) (Kozlowski et al. 1993; Fig. 3). Exposures of Jurassic to Lower Cretaceous Neuquén basin sediments dominate the eastern area; meanwhile, the forelimb of Western Cara Cura exposes high resistant rocks of the Upper Triassic to Lower Jurassic basement (Fig. 3; Fennell et al., 2017). Four short wavelength (<1 km)

anticlines were recognized in the Cara Cura western piedmont, ("western anticlines" 1-4 in Fig. 3a), affecting Upper Cretaceous continental rocks, Quaternary basaltic lavas, and Quaternary fluvial and lacustrine deposits. Structural observations carried out by Fennell et al. (2017) in these Cretaceous-cored anticlines indicate that they are fault-related folds, with a gentle east slope and a steeper front to the west suggesting a west-vergence (Fig. 3c).

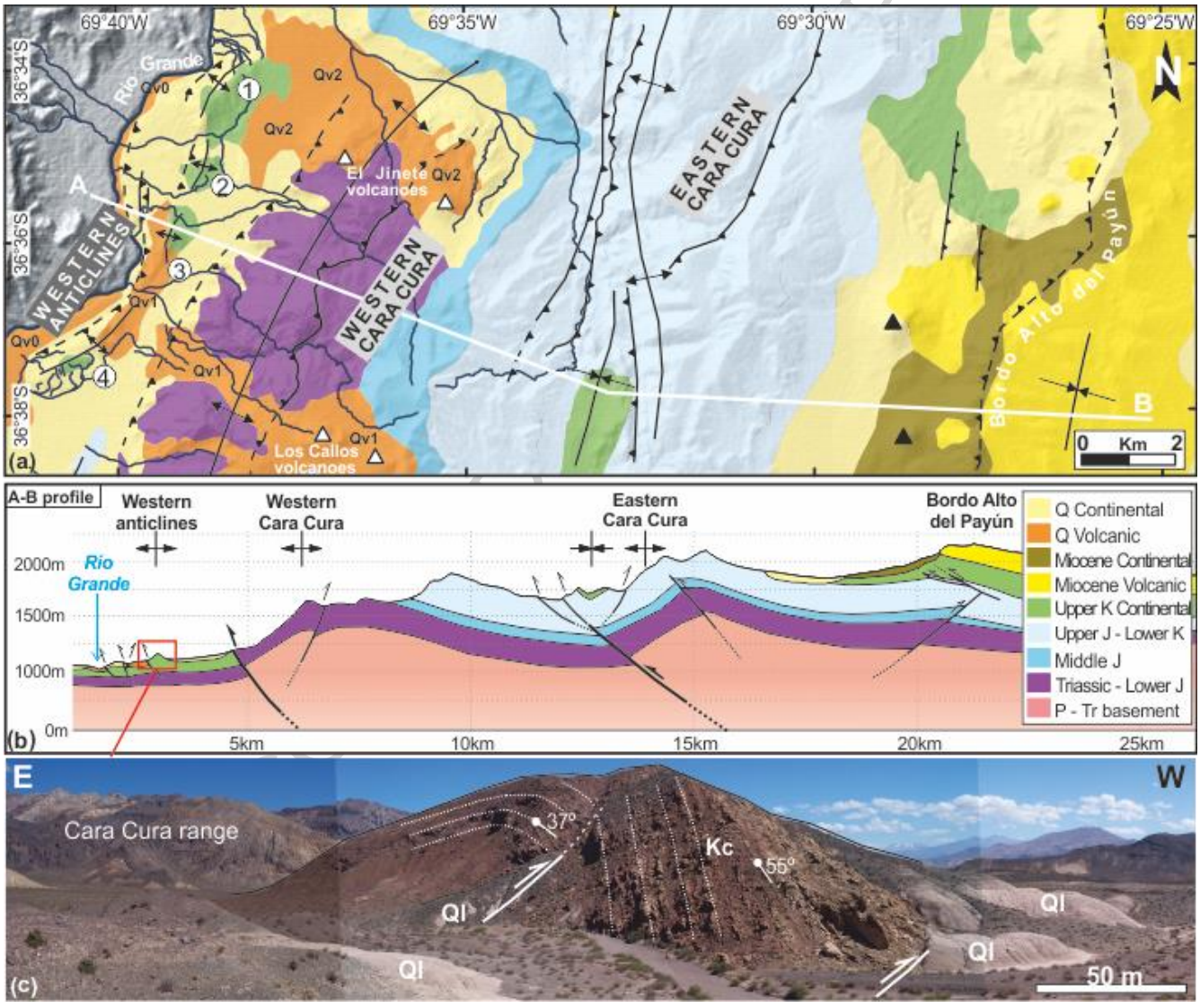

Figure 3*. Geology of Cara Cura range. (a) Structure and main geological units exposed. Short wavelength anticlines to the west of Cara Cura range are numbered from 1 to 4. Geology and structure are modified from Fennell et al. (2017). Location shown in Figure 2a. (b) Structural cross-section A-B.*

In gross lines the two main west-vergent basement faults are highlighted. (c) Structural interpretation for northern tip of Structure 3. References are for both map and section. P: Permian; Tr: Triassic; J: Jurassic; K: Cretaceous; Q: Quaternary; c: continental rocks; l: lacustrine deposits; v: volcanic rocks.

2.2.2 Chihuidos region

South of the Cara Cura range, Chihuidos range, named after Kozlowski et al. (1993), is an 8 km-long monocline limited to the west by a N-S linear scarp with a *ca.* 50 m height (Fig. 4). It should not be confused with the *Dorso de los Chihuidos* high, an important structure located to the south in Neuquén province (Fig. 1; Vergani et al., 1995; Cobbold and Rossello, 2003; Mosquera and Ramos, 2006; Messager et al., 2010, 2014). The Chihuidos monocline is located to the west of a low-relief region, between Cara Cura and Reyes structures, dominated by outcrops of Jurassic and Cretaceous sedimentary rocks (Figs. 2a, 4). Several volcanic dykes have also been described in this region (Guzmán et al., 2011). The Chihuidos monocline is revealed by tilted and folded Upper Miocene sedimentary sequences (Groeber, 1933), equivalents to Pampa del Carrizalito foreland basin deposits (Fig. 4) (Sagripanti et al., 2011).

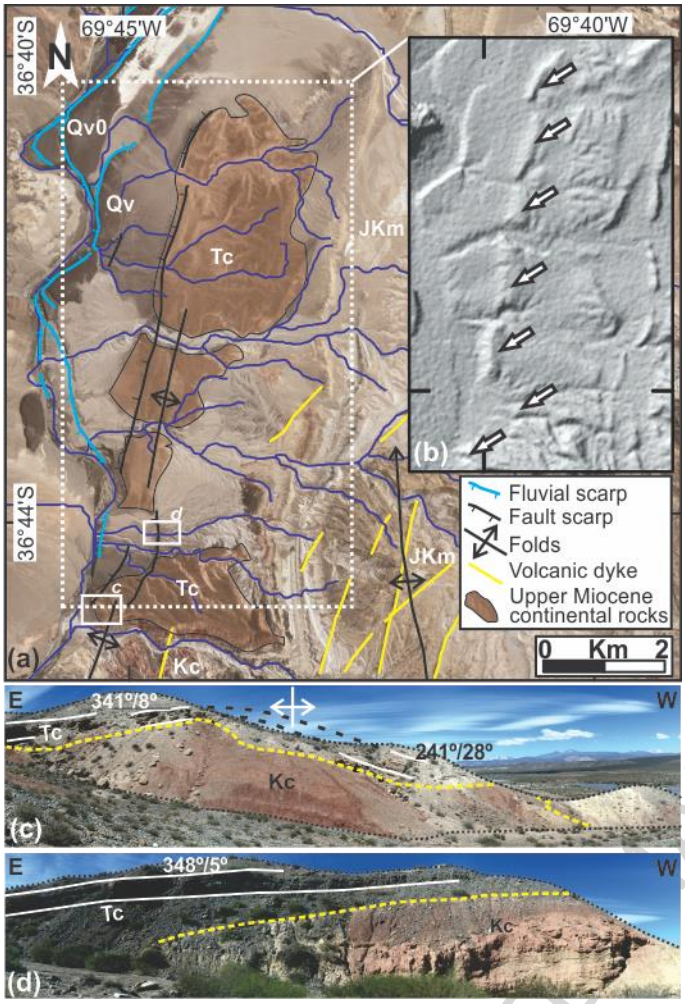

Figure 4. *Geological observations of Chihuidos range. (a) Satellite image of Chihuidos monocline. Main drainage network can be observed as well as the main scarps (fault scarp and terrace risers), also included geological units. Location shown in Figure 2a. (b) Digital elevation model showing the position of Chihuidos range fault scarp (white arrows). (c) Reconstruction of Chihuidos monocline forelimb. (d) Backlimb of Chihuidos monocline with slightly tilted upper Miocene deposits. J-Km: Jurassic-Cretaceous marine rocks; Kc: Cretaceous continental rocks; Tc: Upper Miocene continental rocks; Qv0: Los Volcanes basalts; Qv: Quaternary volcanic rocks (undefined).*

3. Material and methods

3.1 Fieldwork

Fieldwork was carried out in the western slope of Cara Cura and Chihuidos ranges, with particular focus on describing geomorphology and stratigraphic relationships of Quaternary features such as fluvial terraces, lacustrine deposits, alluvial fans, erosional surfaces and different products of volcanic activity. 1:50000 aerial photographs and IKONOS and LandSat7 imagery were employed for the mapping. Stratigraphic relationships were documented in different locations of Cara Cura and Chihuidos areas, to produce a unified Quaternary stratigraphic column. Handheld GPS was used for detailed location and altitude data recovering, particularly regarding knickpoints positions and other geomorphic markers. The top of one particular lava flow affected by Quaternary deformation was sampled for $^{40}Ar/^{39}Ar$ dating. As a complement of field observations, the topographic profiles of the analyzed features were extracted from NASA SRTM 1 arc-second digital elevation data (USGS, 2015).

3.2 Stream analysis

A morphometric analysis was performed to assess whether the tectonic activity has influenced the drainage network and river equilibrium state; however, this analysis should be taken as a first order approach and a complement of geomorphological and geological fieldwork. Rivers play an important role in landscape evolution and, due to their sensitivity to base level changes through time, the analysis of longitudinal stream profiles usually provides information on the balance between uplift and channel incision (Kirby and Whipple, 2001, 2012). Slope breaks or vertical steps in longitudinal profiles indicate a perturbation on the river equilibrium profile or a transient state during which the river adjusts to new conditions (changes in slope, load, discharge, lithology, etc.). These features, defined as knickpoints, can be classified as mobile or fixed regarding their spatial distribution and as climatic, geomorphological, lithological or structural depending on their origin (Wobus et al., 2006; Kirby and Whipple, 2001). Two other parameters were taken into account in the morphometric analysis: concavity (θ) and normalized steepness index (k_{sn}). The former is the rate of change of local slope as a function of increasing drainage area. Under steady state conditions, it usually shows values between 0.3

and 0.6, but if the steady state is interrupted this index may vary: low concavity values are expected in regions under increasing uplift, while higher values appear in sections under decreasing uplift or related to abrupt knickpoints (Kirby and Whipple 2001). At the same time, normalized steepness index is a way to measure the stream gradient, normalized to drainage area, and is generally considered to be directly proportional to tectonic activity or uplift rate (Wobus et al., 2006; Chen et al., 2015). Besides, knickzones were defined as sections of river profiles with high normalized steepness index values (Stolar et al., 2007).

The morphometric analysis was performed in both structures which show similar climatic forcing: arid to semiarid conditions (<200 mm annually; data from http://siat.mendoza.gov.ar/data/search) under which different ephemeral rivers drain from the structures to the allochthonous permanent Río Grande river. The analysis was based on ALOS PALSAR elevation data (downloaded from https://www.asf.alaska.edu) with a pixel size of 12.5 m x 12.5 m. Longitudinal river profiles were extracted using the open-source software TopoToolbox (Schwanghart and Scherler, 2014) while log-log slope-area plots, normalized steepness index and concavity index were calculated from lower order channels in Cara Cura and Chihuidos ranges using the Stream Profiler tool for ArcGIS and Matlab (available at http://geomorphtools.geology.isu.edu/).

4. Results

4.1 Quaternary stratigraphic units from Cara Cura western piedmont

Different locations were surveyed in order to accomplish a Quaternary stratigraphic column from the Cara Cura western piedmont (Fig. 5). The Upper Cretaceous Neuquén Group crops out mainly in the western anticlines (Fig. 3a) and is clearly distinguishable in the field and in satellite images thanks to its reddish color and strong internal deformation.

Covering these rocks, Quaternary volcanic products are spread over the piedmont area. They can be divided into at least three different groups; although multiple eruption events inside each of them

cannot be totally discarded and are difficult to separate. The first two groups are composed of lava flows that descended from El Jinete volcanic center (El Jinete basalts; Qv2) and from Los Callos volcanic centers (Los Callos basalts; Qv1) (Figs. 3, 5). Considering the lateral relationship between Los Callos basalts with other sedimentary units, a sample was taken from these volcanic rocks east of Structure 4 (Qv1), which yielded a whole rock $^{40}Ar/^{39}Ar$ plateau age of 260 ± 70 ka (Fig. 5a and supplementary data). The rocks from El Jinete basalts and their eruptive centers show similar degree of geomorphic preservation than Los Callos basalts suggesting a contemporary origin; although, given their relationships with other Quaternary units it is possible that the rocks from Qv2 might be slightly younger (see Section 4.2). On the other hand, the third group of volcanic rocks comprises a long basaltic lava flow that crops out along the Río Grande river, which can be clearly traced from the northern tip of Structure 1 to the Chihuidos range (Figs. 3, 5). The source of these volcanic rocks is difficult to establish due to fluvial erosion, but remnants of basalts at approximately the same height can be traced further north along the Río Grande river, suggesting that these lavas have flown down from the southern Los Volcanes VF (Fig. 5c). These rocks, grouped as Los Volcanes basalts (Qv0), filled a paleo- Río Grande valley leaving a wide basaltic terrace (S1; Fig. 6c). The base of this unit is only a few meters above the present base level (S0; Fig. 6c) being possible to consider this unit as the youngest of the three. This consideration is in agreement with the young ages obtained for the basalts of Los Volcanes VF that also occupied the Río Grande valley towards the north (25-45 ka; Marchetti et al., 2006; Germa et al., 2010).

Fluvial deposits are widely spread in the area, intercalated with other volcanic and sedimentary units (Figs. 5, 6). They are composed of poorly consolidated and well-selected gravels, with high roundness and a composition mainly of plutonic rocks, andesites and vesiculated basalts, similar to the present alluvium of the Río Grande river, indicating a western provenance from the Main Cordillera. Considering the location of the outcrops along this segment of the Río Grande river, they are interpreted as fluvial terraces remnants (Qf; Fig. 6b). Intercalated with this fluvial unit, between

Structures 2 and 3 (see Section 2.2.1), there is bank of fine siltstones dominated by horizontal lamination, which in some outcrops showed alternation of sand and silt to clay levels and also gypsum intercalations. This unit has a maximum thickness of ~12 m near Structure 3, thinning towards the northwest, and can be interpreted as a playa-lake deposit (Figs. 5, 6e). The reconstruction of the area occupied by these relict lacustrine sediments indicates that the body of water had a surface of at least 0.8 km^2 in the western Cara Cura piedmont zone (Fig. 5a). Along Structures 1 to 3, both fluvial and lacustrine deposits, together with Cretaceous rocks from the Neuquén Group, are beveled resulting in an erosional surface named S2 (Figs. 6d, e). These surface S2 is slightly tilted towards the west and it is between 40 to 80 meters above the present base level (S0; Fig. 6). Lastly, alluvial sediments are widely spread in this piedmont area: those forming the alluvial plain of water courses that descend from Cara Cura range and cover the present piedmont floor; those that form part of the inactive alluvial fans, developed between the Cara Cura mountain front and the western structures; and, those that form a thin alluvial cover the erosional surface S2 to the west of Structures 1 to 3 (Fig. 6e). These units are mainly composed of poorly rounded clasts of mainly Triassic volcaniclastic rocks and Neuquén basin calcareous rocks, suggesting a local provenance from the Cara Cura range.

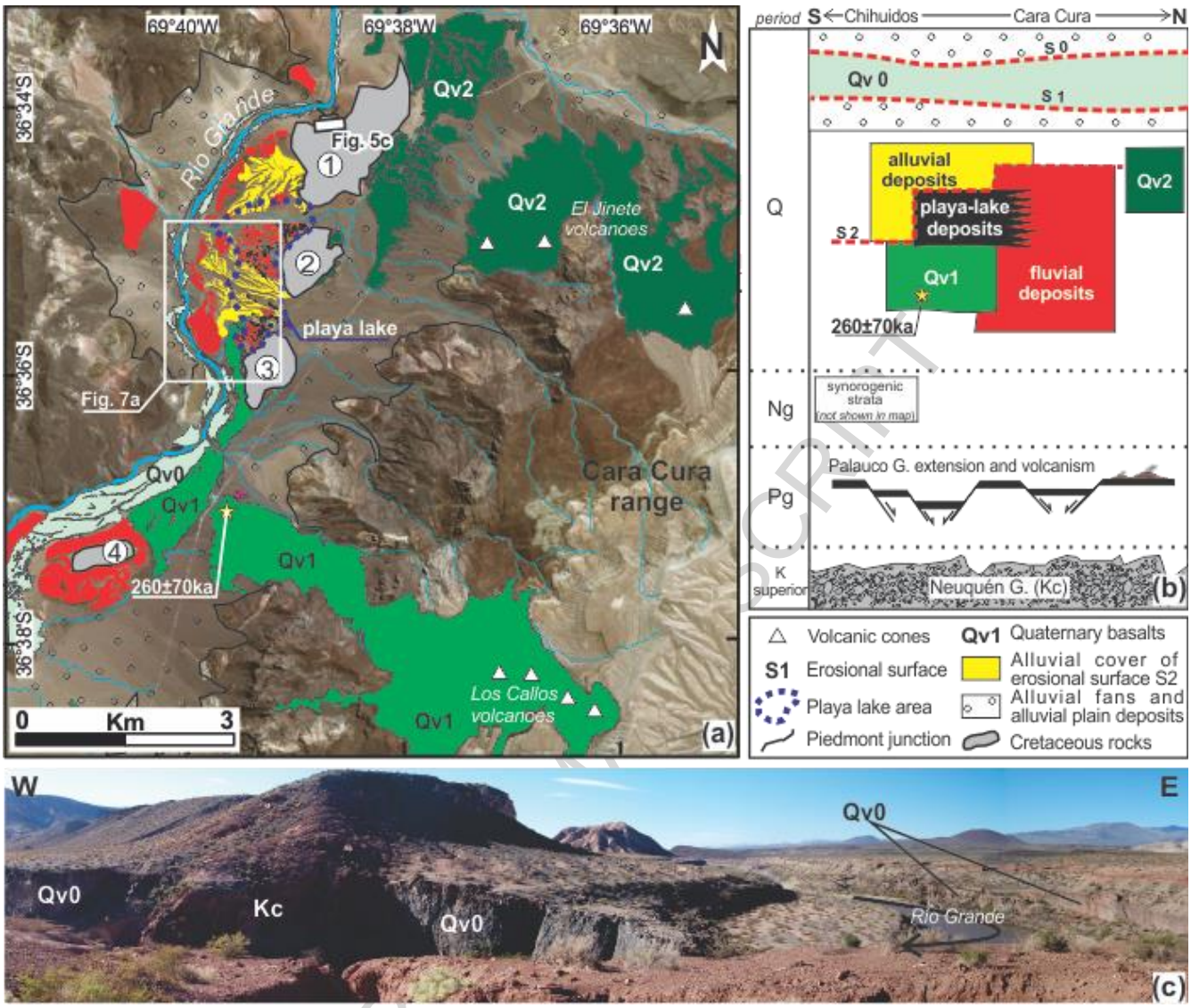

Figure 5. *Quaternary geology of Cara Cura range western slope. (a) Geologic map with main Quaternary units. The location of a $^{40}Ar/^{39}Ar$ age presented in this work is indicated with a yellow star. Numbers in white circles refer to western anticlines, Structures 1 – 4. Blue dashed line corresponds to the area with playa-lake deposit outcrops. (b) Stratigraphic column of Cara Cura and Chihuidos areas. Colors correspond to the geological units of Figure 5a. References for both figures are indicated. (c) Field photograph corresponding to Los Volcanes basalts (Qv0) affected by fluvial erosion at the northern tip of Structure 1.*

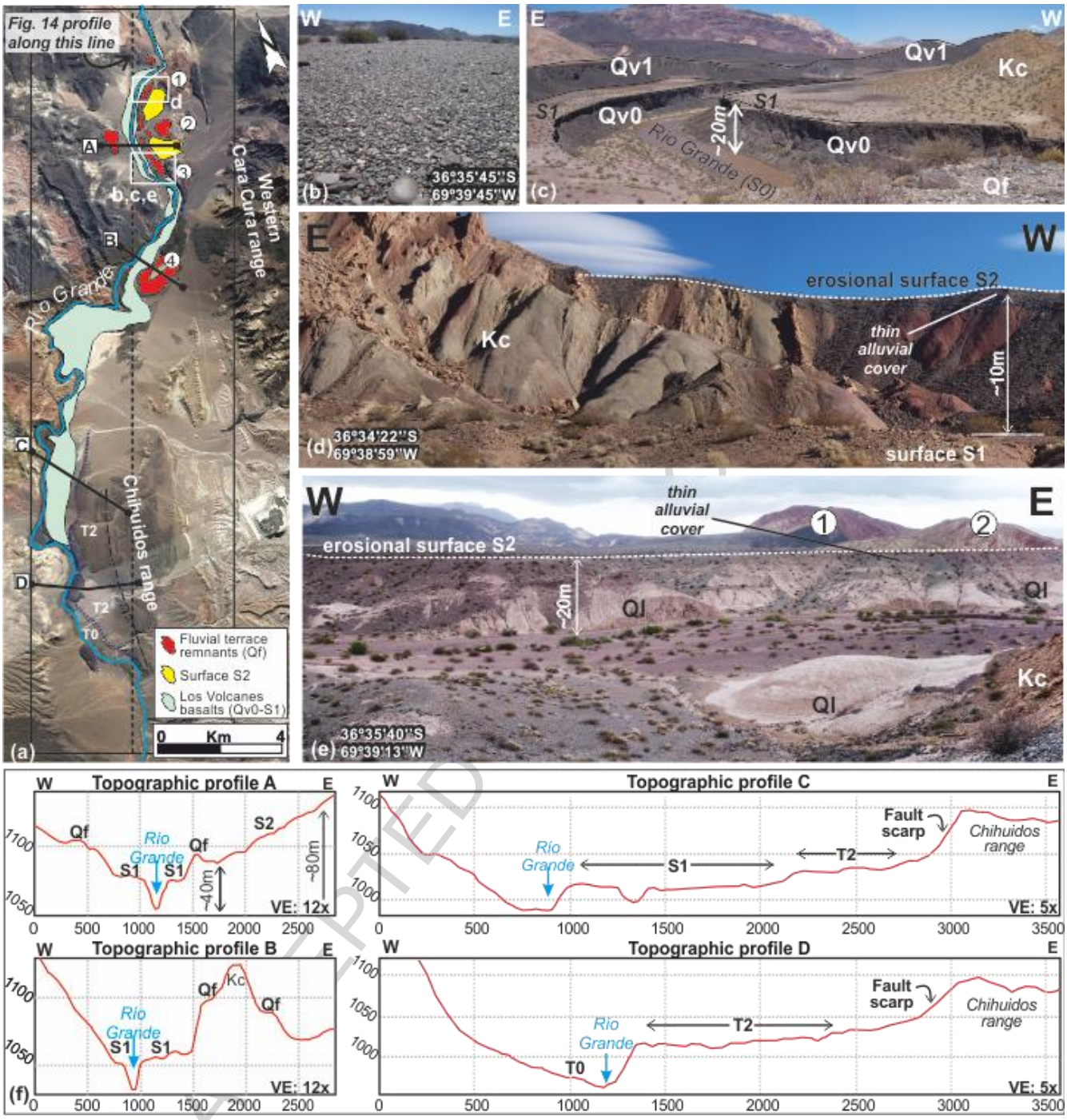

Figure 6. *(a) Satellite image showing the distribution of fluvial terrace remnants (Qf), Los Volcanes basalts (Qv0), erosional surface S2 along the Río Grande valley at Cara Cura segment and terraces T0-T2 at Chihuidos segment. Location of topographic profiles A – D is indicated. Numbers in white circles refer to the western anticlines. White squares correspond to the other figures' location. (b) Surficial aspect of the fluvial terrace remnants. (c) Field photograph taken from the same location as*

Figure 6b. A ~20 m incision over Los Volcanes basalts (Qv0) can be seen. (d)Example of erosional surface S2 beveling Cretaceous rocks (Kc). A ~10m relief with respect to surface S1 is indicated. (e) Example of erosional surface S2 beveling lacustrine deposits. A ~20 m relief with respect to surface S1 is indicated. (f) Topographic profiles A and B, transverse to Río Grande river at western Cara Cura piedmont, and C and D, transverse to Río Grande river at Chihuidos range; S1 and T2 correspond to different basalt terrace levels. T0 corresponds to the lowest fluvial terrace. Profile units are in meters in both axis. VE is vertical exaggeration. (See text for further details)

4.2 Morphostuctural analysis in Cara Cura range

To the west of Structures 2 and 3, the surface S2 dips towards Río Grande river, limited by outcrops of the fluvial terrace remnants which depict two small bulges (Profile A in Figure 6f, Fig. 7). The internal structure of one of these bulges, the eastern one, is exposed by the erosion of an ephemeral water course that reveals Quaternary fluvial and alluvial conglomerates covered by a 2 m-thick fine sand reddish bank with horizontal lamination and a slight inclination towards the east, which thins towards the west (Fig. 7c). The origin of these sand deposits is uncertain, but, given its color, this bank may be the product of the erosion of Neuquén Group rocks. This sedimentary sequence is clearly affected by two east-vergent faults that displace the reddish bank *ca.* 2 and 3 m respectively (Fig. 7c). A main west-vergent fault can also be interpreted despite its fault plane is not clear due to the detritus cover (Fig. 7c). The sedimentary sequence (fluvial conglomerates and the fine sand deposits above them) can be correlated in the hanging wall and in the footwall of these fault (Fig. 7c); and, although a river bank collapse may produce similar displacement features, according to the topographic profiles in Figure 7b the eastern bulge presents a morphologic expression that can be potentially associated with an east dipping main-structure with a N-S trend, like the one here interpreted. Under this consideration, the fluvial conglomerates, composed of coarse boulders and gravels of granitic, volcanic and metamorphic rocks, would be displaced by the west-vergent N-S main reverse fault for at least 7 m,

which is approximately the vertical uplift observed for the eastern bulge in profiles P2 and P3 from Figure 7b. To the top, the sequence is partially covered by alluvial sediments with horizontal lamination which are only displaced at their lower levels (Fig. 7c). This faulted sequence is considered a direct evidence of Quaternary deformation, due to the poor consolidation of the fluvial deposits and their lateral relationship with Pleistocene lava flows.

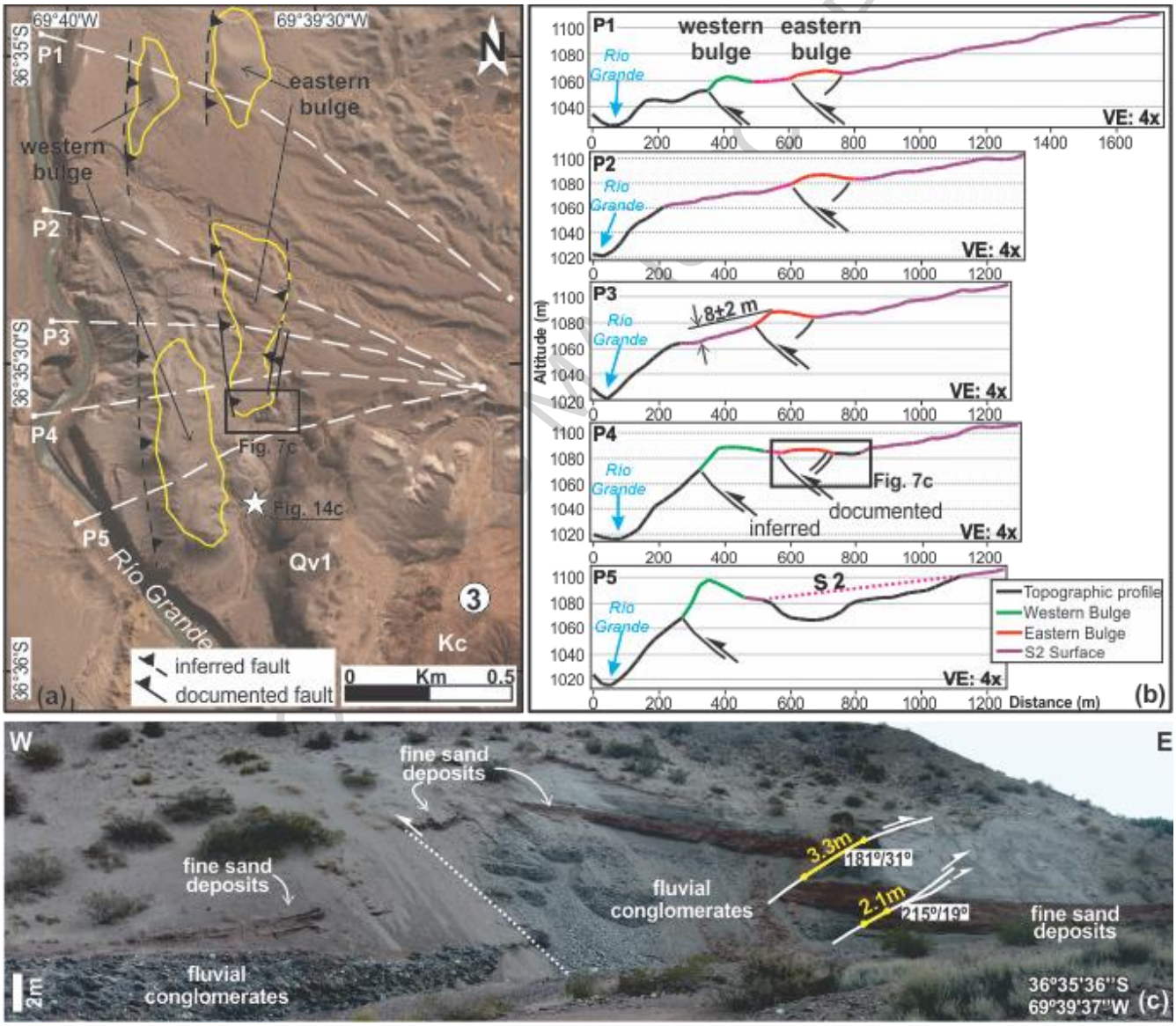

Figure 7*. Evidences of Quaternary faulting. (a) Satellite image showing western and eastern bulges (yellow contours), the structural interpretation for this area and the location of P1-P5 topographic*

profiles. Location shown in Figure 5a. Kc: Cretaceous continental rocks; Qv1: Los Callos basalts. Number in white circle indicates Structure 3. Black square corresponds to the location of Figure 7c. (b) Topographic profiles P1-P5. Structures are interpreted from topography, except documented faults in profile P4. References for line colors are included. VE is vertical exaggeration. (c) Field picture showing a set of reverse faults affecting Quaternary strata. The west vergent fault plane is interpreted from the relationship between fluvial conglomerates and fine sand deposits (see text for further details).

In some locations, the outcrops of the playa-lake deposit are tilted. In the forelimb and backlimb of Structures 2 and 3 they dip 18º to NNW and 20º to E respectively (Fig. 8). Moreover, in the northern tip of Structure 3, lacustrine deposits dip 16º to E and 78º to W, depicting an anticline shape with western vergence and a NW hinge trend (N15ºW) (Fig. 8). Despite no surface expression associated with these structures was observed, tilted and faulted strata can be considered as direct neotectonic evidence, suggesting that part of the Quaternary uplift of Structures 2 and 3 was transferred to the sedimentary cover. Timing of these deformation is not entirely clear, but the tilted playa-lake deposits in the forelimb of Structure 2 appears to be capped by El Jinete basalts (Qv2), which do not show evidence of being deformed (Fig. 8b). Although no age constraint is available for this volcanic unit, deformation in this sector should be older than El Jinete basalts.

Horizontal lamination prevails in these outcrops, however many of them show internal deformation as convolute lamination, dish and pillar, diapirs and low-angle faulting (Fig. 9). Although a more detailed analysis would be needed in order to define them as seismites, their presence is suggestive being potentially associated with local ground-shaking.

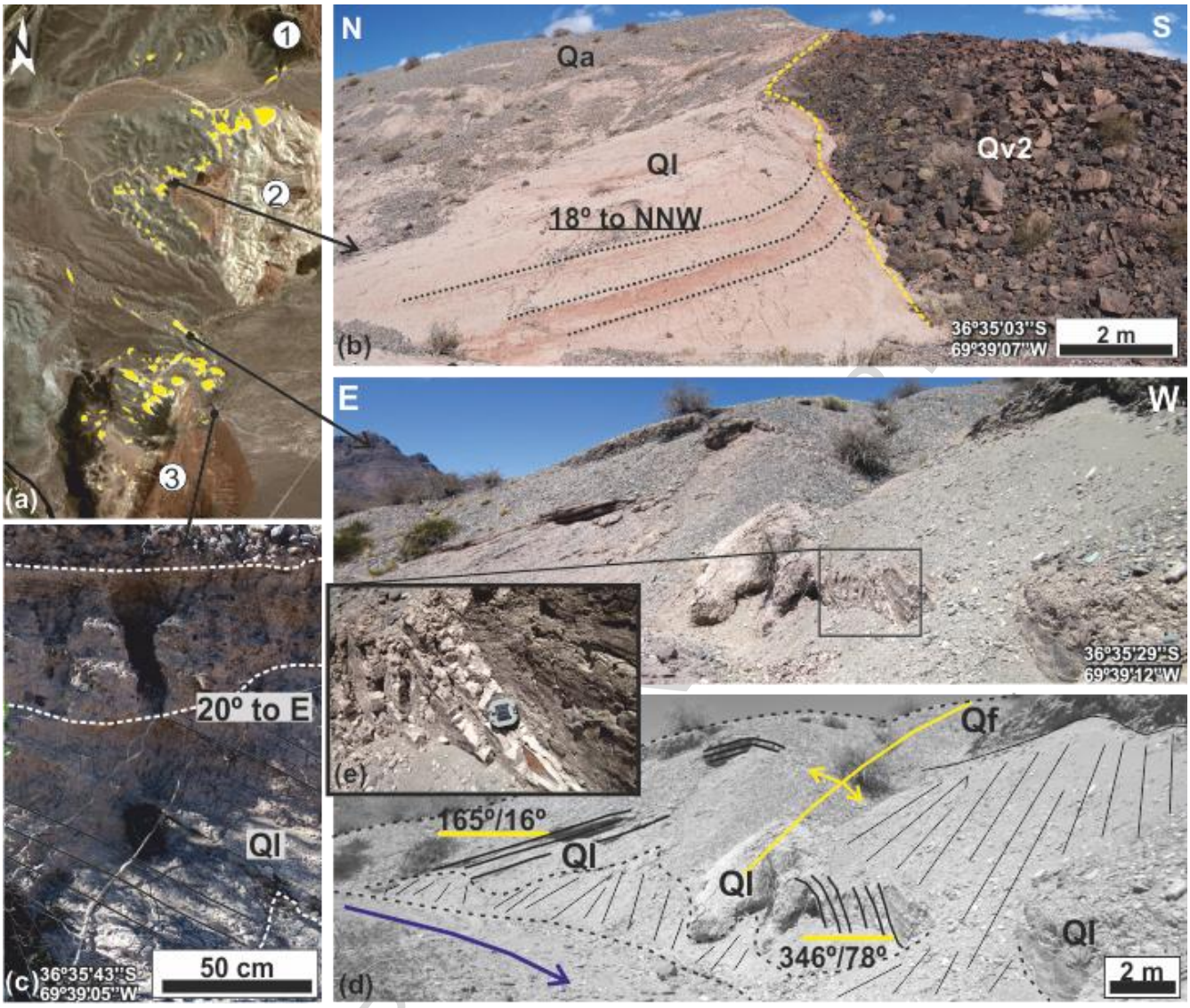

Figure 8. *(a) Playa-lake deposits scattered through Cara Cura western slope (in yellow). White circled numbers refer to the western anticlines. (b) Lacustrine strata tilted 18º to NNW, covered by alluvial deposits and a basalt flow. (c) Tilted lacustrine beds covered by gravels and alluvial deposits. (d) Field photo and interpretation of folded and faulted lacustrine benches covered by fluvial gravels. (e) Detailed photo of the vertical benches from the forelimb. Ql: lacustrine; Qv2: El Jinete basalts; Qa: alluvial; Qf: fluvial.*

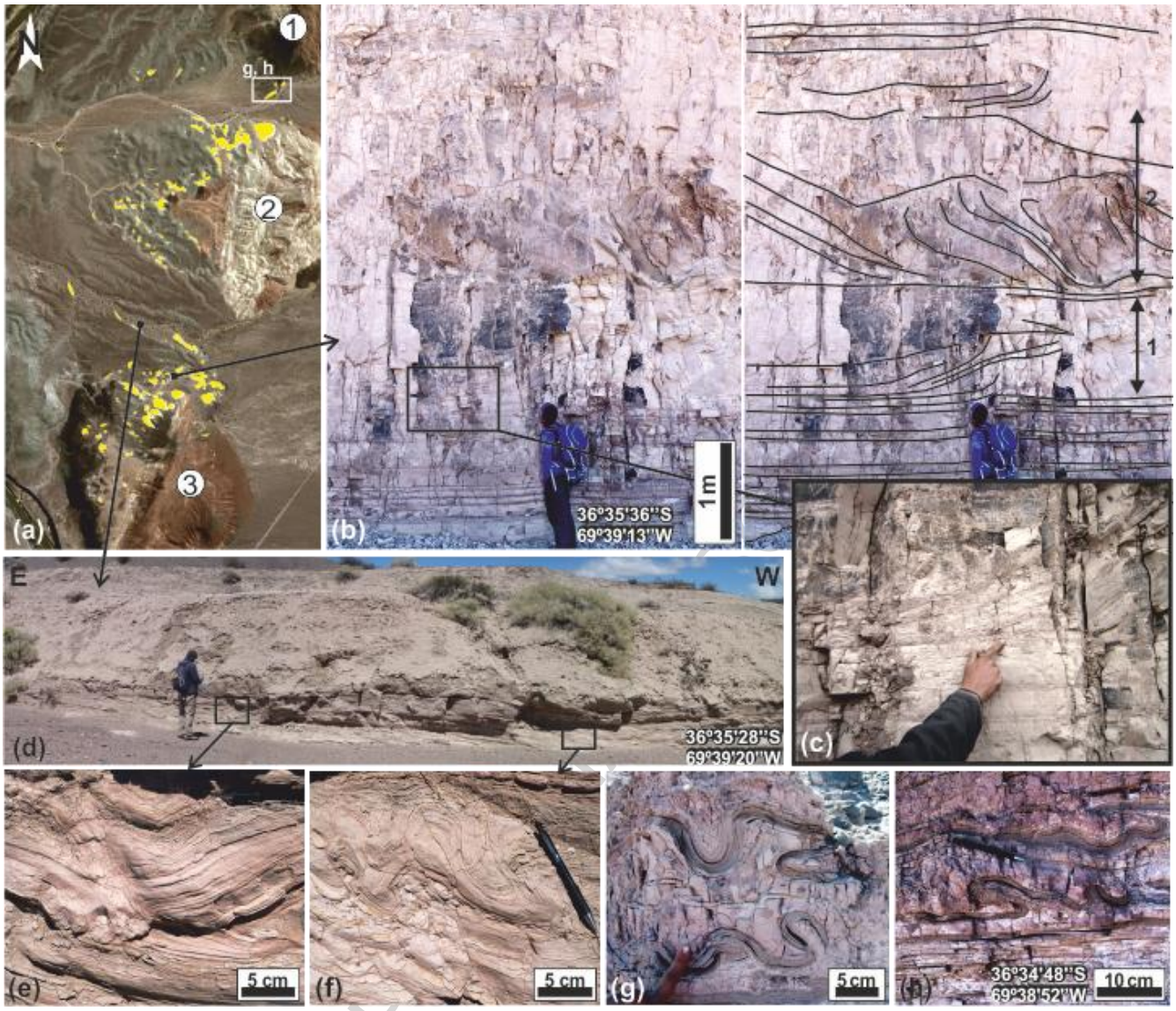

Figure 9. *Evidences of soft sediment deformation. (a) Playa-lake deposits scattered through Cara Cura western slope (in yellow). White circled numbers refer to the western anticlines. (b) Lacustrine sediments outcrop, with horizontal lamination at the bottom and top, and two levels (1 and 2) with convolute and chaotic stratification. (c) Detail picture from the contact between undeformed and deformed levels. (d) Lacustrine deposits outcrop showing internal deformation. (e) Intrasedimentary fault affecting slightly folded levels. (f) Convolute lamination, pencil as scale. (g) and (h) Convolute lamination in an outcrop at the south of structure 1 (location in Fig. 9a; GPS location is almost the same for both pictures).*

Towards the south, at Structure 4, Los Callos basalts (Qv1) act as a geomorphic marker for Quaternary deformation (Fig. 10). This lava flow reaches the western piedmont occupying a region between Structures 3 and 4 (Figs. 5, 10). It is partially covered by the alluvial fans but, in its distal segment, depicts an anticline shape, whose N-S hinge has a ~80 m relief (Fig. 10f). In this segment, a set of parallel NE-SW cracks was observed (Fig. 10b). In the northern tip of Structure 4, the observed relief is much lower, *ca.* 10 m (Fig. 10). There, a fluvial channel exposes the internal structure of the basalt, from which a gentle backlimb and a steeper forelimb were interpreted, coincident with a west-verging anticline structure (Fig 10c). The lava flow is in a lateral relationship with fluvial conglomerates, which also seem to be folded (Fig. 10e). A 50-m height scarp clearly seen in topographic profile B (Fig. 6f), limits to the west the Structure 4 (Fig. 10d). Along this scarp two watergaps are developed, one above the basalts and the other in the contact between the basalts and the fluvial deposits (Fig. 10d). This same scarp is associated to a broom shape pattern between Structures 3 and 4 (Fig. 10a).

In the axial zone of the Structure 4 an 80 m maximum uplift was measured (Fig. 10f). Meanwhile, the 10 m relief, observed in the northern tip of Structure 4, can be considered as a minimum uplift (Fig. 10c). From the $^{40}Ar/^{39}Ar$ analysis, Los Callos basalts' maximum and minimum age can be constrained between 190 ka and 330 ka (see Section 4.1). Then, crossing maximum uplift with minimum age values and vice versa, the maximum and minimum uplift rates obtained for the surface of the axial zone of Structure 4 are 0.4 mm/yr and 0.03 mm/yr respectively. Uplift rates (U) can be converted into slip rates (S) considering $S = U/\sin d$, being d an average reverse fault angle of 30º, sustained by a similar fault dip angle from the retrowedges found in the eastern bulge (Fig. 7c). Then, maximum and minimum slip rates obtained are 0.8 mm/yr and 0.06 mm/yr respectively.

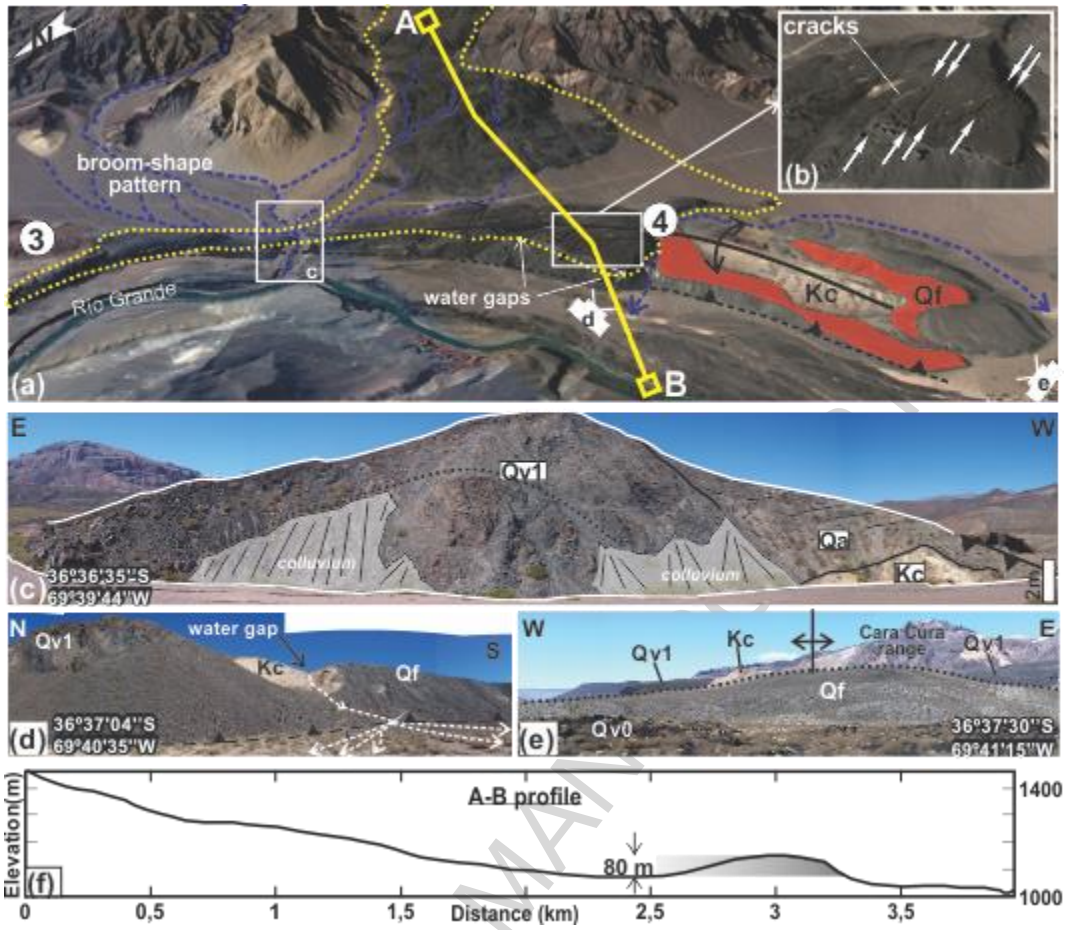

***Figure 10**. Detail of Structure 4. (a) Oblique Google Earth view of Structures 3 and 4. Los Callos basalts (yellow dashed line) spread over the piedmont, being affected by a blind west vergent thrust. White squares and camera drawings indicate other figures' location. (b) Longitudinal cracks at the anticline hinge of Structure 4 indicated by white arrows as a consequence of folding stresses. (c) Northern tip of Structure 4. Dashed line corresponds to the interpreted internal structure. (d) Frontal scarp of Structure 4. A watergap can be seen, coincident with the lateral contact between Los Callos basalts (Qv1) and fluvial terrace deposits (Qf). (e) Field photograph taken from the south of Structure 4 showing fluvial terrace deposits slightly folded. (f) Topographic profile as showed in Figure 10a. Shadowed area corresponds to the surface expression of Structure 4 over Los Callos basalts.*

4.3 Morphometry of the western Cara Cura piedmont

A morphometric analysis was performed in the Cara Cura range considering that erosion/deposition conditions in this region may have obscured major surface evidences, as geomorphological observations showed. This first order approach to river dynamics in Cara Cura western piedmont revealed some interesting characteristics. Two bigger sub-basins (I and III) and a smaller one (II) are developed in the piedmont zone (Fig. 11a).

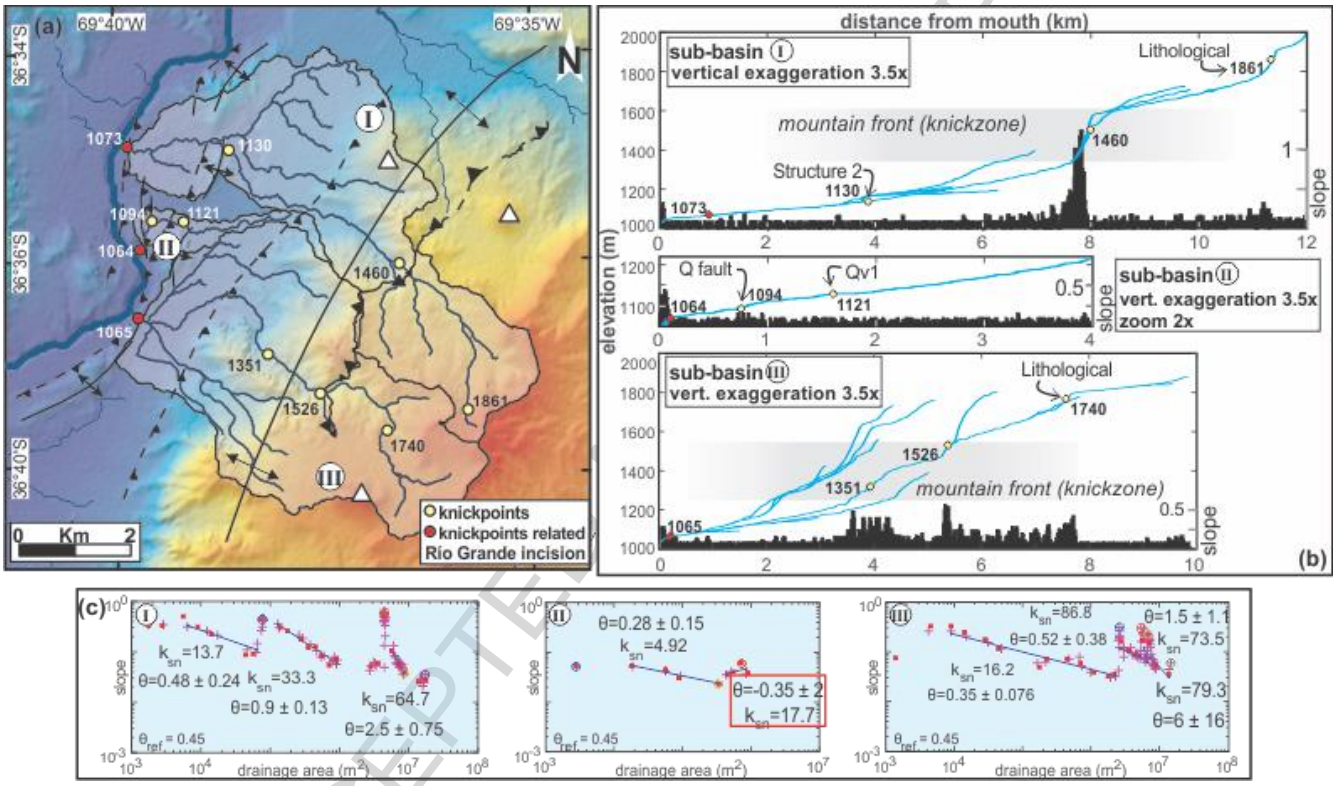

Figure 11. *Morphometry of Cara Cura range western rivers. (a) Digital elevation model with the three drainage sub-basins analyzed and location of knickpoints; white/black numbers refer to their height in meters. Geological structures are also plotted. (b) Longitudinal stream profiles of sub-basins I to III. Knickpoints or knickzones (shadowed) associated features are indicated. (c) Log-log slope vs. area plots. Red square highlights a segment in river II with predominantly negative concavity values, coincident with the fault zone segment.*

Longitudinal stream profiles in the two largest networks present outstanding profile breaks conditioned by the hard lithology of Triassic to Lower Jurassic rocks that dominate the mountain front of Cara Cura range, mainly composed of acid breccia, ignimbrites, conglomerates and sandstones (Figs. 3, 11b). The slope vs. area plots show that these steps in the longitudinal profiles are related to segments with very high k_{sn} values (k_{sn}: 33.3/64.7 and 86.8/73.5/79.6 for rivers I and III respectively, Fig. 11c), thus being possible to define them as knickzones. Those knickpoints at 1861 m and 1740 m height, belonging to the headwaters, are related to a lithological change between Middle Jurassic and Triassic to Lower Jurassic sedimentary units (Fig. 3). Downstream, the segment of rivers I and III that runs through Cara Cura western structures appears to have concave-up shape with no disruptions. However, in sub-basin I, a minor knickpoint was observed at around 1130 m, coinciding with the trace of a fault that controls the western anticlines (Fig. 11).

The sub-basin II is considerably different from the previous ones. It is only composed of a 4 km length trunk river with no tributaries. Its longitudinal stream profile does not show any major knickpoint but at least two minor knickpoints can be highlighted where concavity changes define a convex-up segment (plot II in Fig. 11b). While the knickzones in sub-basins I and III may correspond to Cara Cura mountain front, the two knickpoints of this particular sub-basin are related to both a change from graded plain to basaltic bedrock plain (Qv1) and to the fault zone described in the previous section (plot II in Fig. 11b). Log slope vs. log area relationship for this sub-basin (Plot II in Fig. 11c) shows that the concavity values (θ) are predominantly negative (θ: -0.35 ± 2) indicating a convex profile, unlike the rest of the cases where positive values corresponded to concave-up profile segments.

4.4 Chihuidos region

At least three terrace levels were observed, from which two of them may have partially developed as basalt terraces (S1 and T2), formed as a consequence of lava flows filling the Río Grande valley

followed by a stage of fluvial incision and the youngest (T0) corresponds to a fluvial terrace (Figs. 6a, 12). Running N-S in the western limb of the Chihuidos structure, an 8 km-long scarp is developed (Fig. 4). This scarp is approximately 50 m high and is coincident with a west-vergent fault revealed by exposures of Cretaceous Neuquén Group rocks (Figs. 4, 6f, 12). Together with a short linear scarp to the west, both can be classified as residual fault scarps, considering that primary tectonic surface is completely degraded (Stewart and Hancock, 1990). Incision anomalies, minor creeks and scarp-parallel rivers are developed over these vertical steps (Fig. 12c).

From a satellite image interpretation and field work it was observed that the alluvial Neogene cover of the Chihuidos structure is slightly tilted to the east (Fig. 12d). These deposits reach 80 m in thickness and are separated from the Cretaceous rocks by an erosional unconformity (Fig. 12e).

The drainage network was analyzed in order to understand the interaction of fluvial processes with the structure. Four ephemeral streams cut across this structure in an E-W direction (Fig. 12). The relief and incision degree of the rivers increases towards the south, with strong differences between northern and southern drainage sub-basins. Streams I and II have smaller basins and show almost no incision, contrarily to both streams III and IV that show elongated and more extensive basins with higher degree of incision, as revealed by thick exposures of Neogene and Cretaceous rocks (Figs. 4c, d), river gullies and an entrenched meander in the southern tip of the range (Fig. 12c). Streams III and IV also showed an increase in their sinuosity, when running through the Chihuidos range (Fig. 12c). These differences between northern and southern basins can be adjudicated to the emplacement of the basalts in Río Grande valley, at the northern segment of Chihuidos range (Fig. 4). Thus, due to their resistance to erosion the basalts may have temporarily increased the base level for streams I and II, diminishing their vertical incision capability. However, a higher cumulated uplift in the southern portion of the Chihuidos range may have had the same consequences, increasing the vertical incision power in streams III and IV.

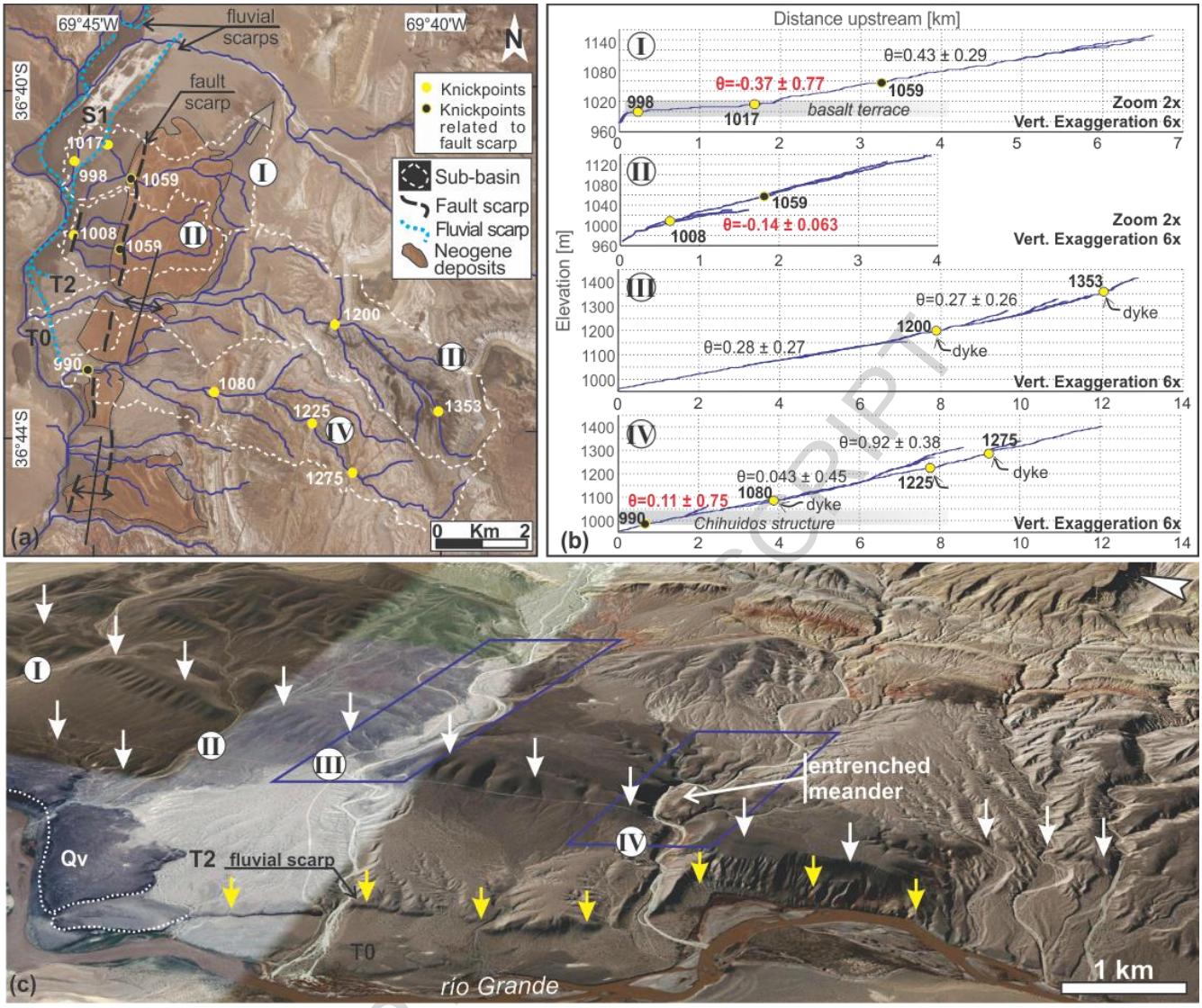

Figure 12. *(a) Satellite image of the Chihuidos range. Main drainage sub-basins are highlighted in white dashed lines. River network is shown together with the main scarps that limit the Chihuidos structure to the east. (b) Longitudinal river profiles of the four basins indicated in Figure 12a. Red concavity values indicate almost convex or convex segments. (c) Oblique Google Earth view of the range, where white arrows indicate the position of the two fault scarps and blue squares highlight river segments of higher sinuosity.*

Longitudinal stream profiles were obtained from the four main rivers that cut across Chihuidos monocline (Fig. 12b). These profiles do not show the typical concave-up shape, having some of them

even convex-up shapes, as indicated by concavity index values (Fig. 12b). Stream I, for instance, presents an upstream convex-up segment, while stream II longitudinal profile shows two segments with convex-up shape and two knickpoints (Fig. 12b). The convex-up segments of both streams coincide with T2 terrace level. However, the knickpoints in both streams (at 1059 m) coincide with the main scarp of the Chihuidos structure and the one at 1008 m in stream II is coincident with a frontal scarp to the west of the main scarp, signaled by small parallel incisions (Fig. 12b). The convexity on river profiles in these cases can be explained partially due to the restricted drainage area of these channels, thus the lower capability of the stream to erode over basalt terrace T2 and achieve equilibrium. A different situation is observed for stream III, where convex-up shape is not as clear as for the first two channels, and two knickpoints can be identified, although corresponding to the intersection of the stream with a volcanic dyke and not with a neotectonic structure (Fig. 12). The three knickpoints located in the upper segments of stream IV also respond to a volcanic dyke. Meanwhile, the knickpoint located downstream is coincident with the main residual fault escarpment (at 990 m; Fig. 12).

5. Discussion

5.1 Proposed landscape evolution of Cara Cura western piedmont

In Figure 13 we present a landscape evolution proposal for Cara Cura western piedmont, following the stratigraphic column and field observations (Figs. 5, 6). This geomorphic evolution proposal clearly shows that, along the studied segment, the Río Grande have had a complex geomorphic history comprising different stages of fluvial incision, lateral erosion and aggradation during middle to late Pleistocene (Fig. 13). A more detailed chronology of the different elements (volcanic units, fluvial terraces and strath or erosional surfaces) will be necessary to address the forcing behind those changes but, as a preliminary attempt, some important inferences can be made in relation to the interplay between Quaternary tectonics, volcanism and fluvial processes.

As described before, the basement of this region is formed by the Cretaceous Neuquén Group, which forms the core of the western anticlines. These anticlines probably acted as topographic highs since the Miocene contractional stage that affected the Malargüe FTB, this scenario may be considered as the initial stage (Stage 1 in Fig. 13).

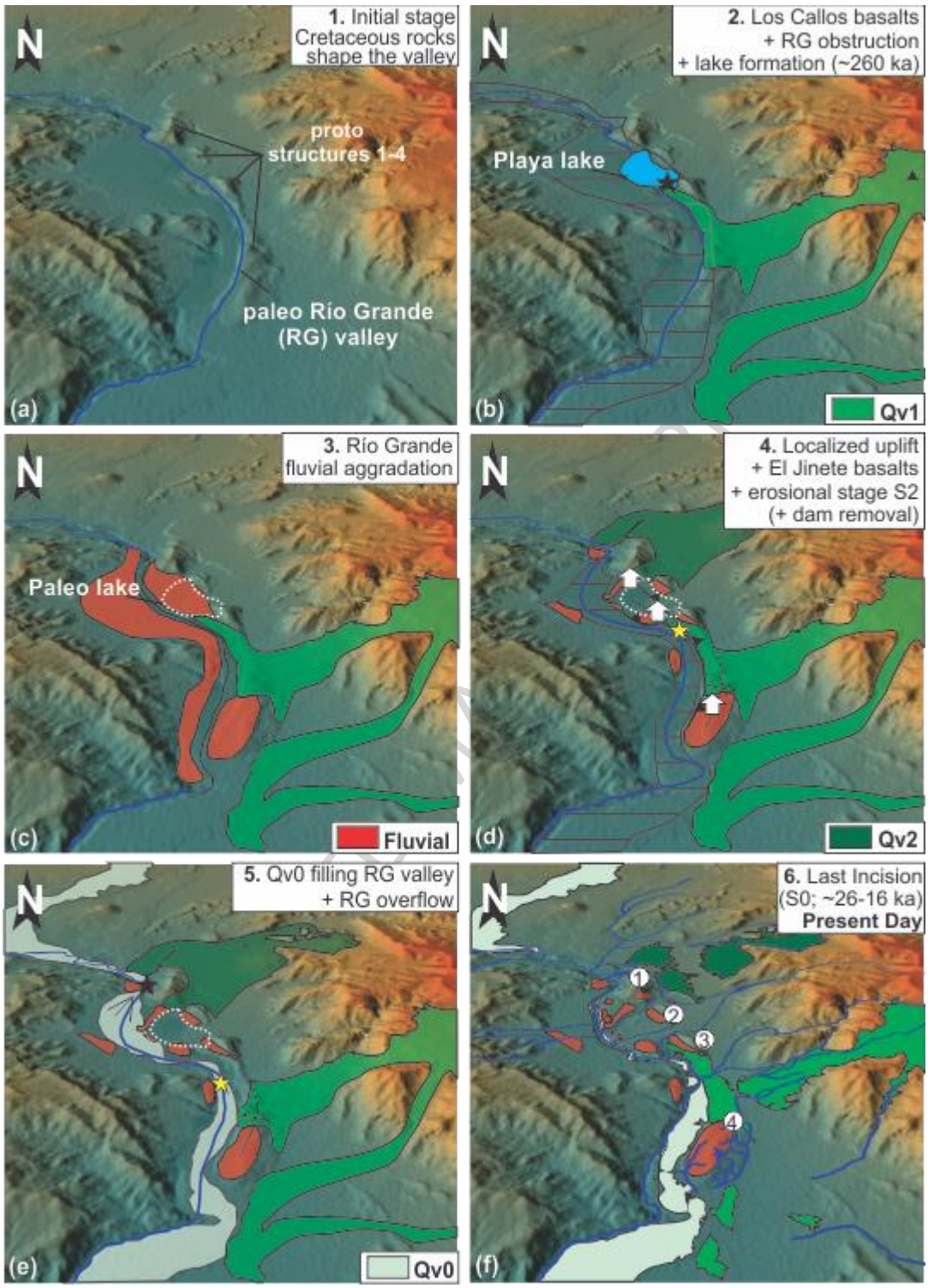

Figure 13*. Proposed schematic evolution of Río Grande river segment to the west of the Cara Cura range (see text for further details). Six stages are proposed (1 to 6), the last corresponding to present day conditions. Locations where Río Grande was blocked (black stars) and where dam removal was initiated (yellow stars) are indicated. White arrows in Stage 4 correspond to structures where*

Quaternary uplift was interpreted. Dashed area in captions a, b and d refer to the width of the paleo-Río Grande valley. Numbers in white circles in caption f correspond to the western anticlines (see text for further details).

It has been observed in different rivers around the world that lava flows causing volcanic dams can have an important effect on the fluvial systems upstream and downstream the blockage (e.g. Veldkamp et al., 2012; van Gorp et al., 2013). In Cara Cura region, at least two potential damming events were identified. The first is associated with the middle Pleistocene basalts descending from Los Callos volcanic centers (Qv1) which may have produced the small playa-lake at Stage 2 of the proposed scheme (Fig. 13). The roundness and composition of the fluvial conglomerates that cover these lacustrine deposits indicate a provenance from the Main Cordillera being possible to interpret that fluvial aggradation occurred despite the Río Grande river was still partially dammed (Stage 3 in Fig. 13). Then, the river was reconnected with its downstream segment (Stage 4 in Fig. 13). A chaotic deposit with large basaltic and lacustrine boulders in front of Structure 3 could be indicating the reconnection of paleo Río Grande river (Fig. 14c). This reconnection may have induced erosional conditions in the western Cara Cura piedmont (Stage 4 in Fig. 13) as recorded in the erosional surface S2 that affects Cretaceous rocks, the basalts and the fluvio-lacustrine sedimentary sequence along Structures 1 to 3 (Fig. 6). It is important to note that the thin bed of alluvial sediments of local provenance that covers this surface may be indicating that the tributary channels were the responsible for its formation and not the Río Grande river. The development of this surface might have been somehow coeval with the localized uplift in the western piedmont of Cara Cura range (Stage 4 in Fig. 13), which may have favored the formation of this type of erosional surface at the western slope of the Structures 1 to 3. In some areas the cumulated uplift may have been higher than others preventing erosion to wipe out the fluvial sediments. The case of the eroded deformed lacustrine sediments in Figure 8b illustrates the case of erosion being higher than uplift. Meanwhile, in the case of the western

bulge and the Structure 4 the fluvial terraces were preserved (Figs. 6, 10). As Figure 3 suggests, the western anticlines may be controlled by an almost N-S blind thrust, with a detachment level in Cretaceous sedimentary rocks. However, this reactivation may have not be the same all along this west-vergent thrust, which could explain the higher uplift of western bulge compared to the eastern bulge or the lack of topographic signature for the folded lacustrine deposits (Figs. 7, 8). At this stage, the base level should have been higher than present allowing the lateral erosion from the tributary channels to occur. Then a base level fall, of more than ~20 m may have taken place to develop the paleo Río Grande valley before Stage 5 (Fig. 13e). At this stage the second damming event might have occurred. It belongs to the most recent lava flows located along Río Grande valley that may have produced a blockage to the north of Structure 1 (Stage 5 in Fig. 13). The presence of fluvial features (distributary patterns, paleo-channels) on top of this volcanic unit (Figs. 14d, e) suggests that being the Río Grande river partially or totally dammed, some pouring occurred over the volcanic rocks before the river was finally capable to incise them (Figs. 6c, 13f). Subsequently, the reconnection of the fluvial system might have begun between the Structures 3 and 4, where a collapse of the lava walls and an epigenetic gorge are observed (Figs. 14e, f). Downstream this point, the river runs in the western margin of Los Volcanes basalts (Fig. 6) and is eroding softer rocks (Cretaceous sedimentary rocks mainly); small fluvial terraces are observed in this region (Fig. 14e). At the same time, it is possible to infer that once the dam was started to be removed, Río Grande river experienced the vertical incision observed upstream, up to the northern tip of Structure 1 (Fig. 14d). Available ages of lava flows that obstructed Río Grande river in Los Volcanes region, further north, indicate that a similar incision event might have occurred between 26 and 16 ka (Marchetti et al., 2006; Germa et al., 2010). However, regional correlations are difficult to assess with this type of landscape dynamics.

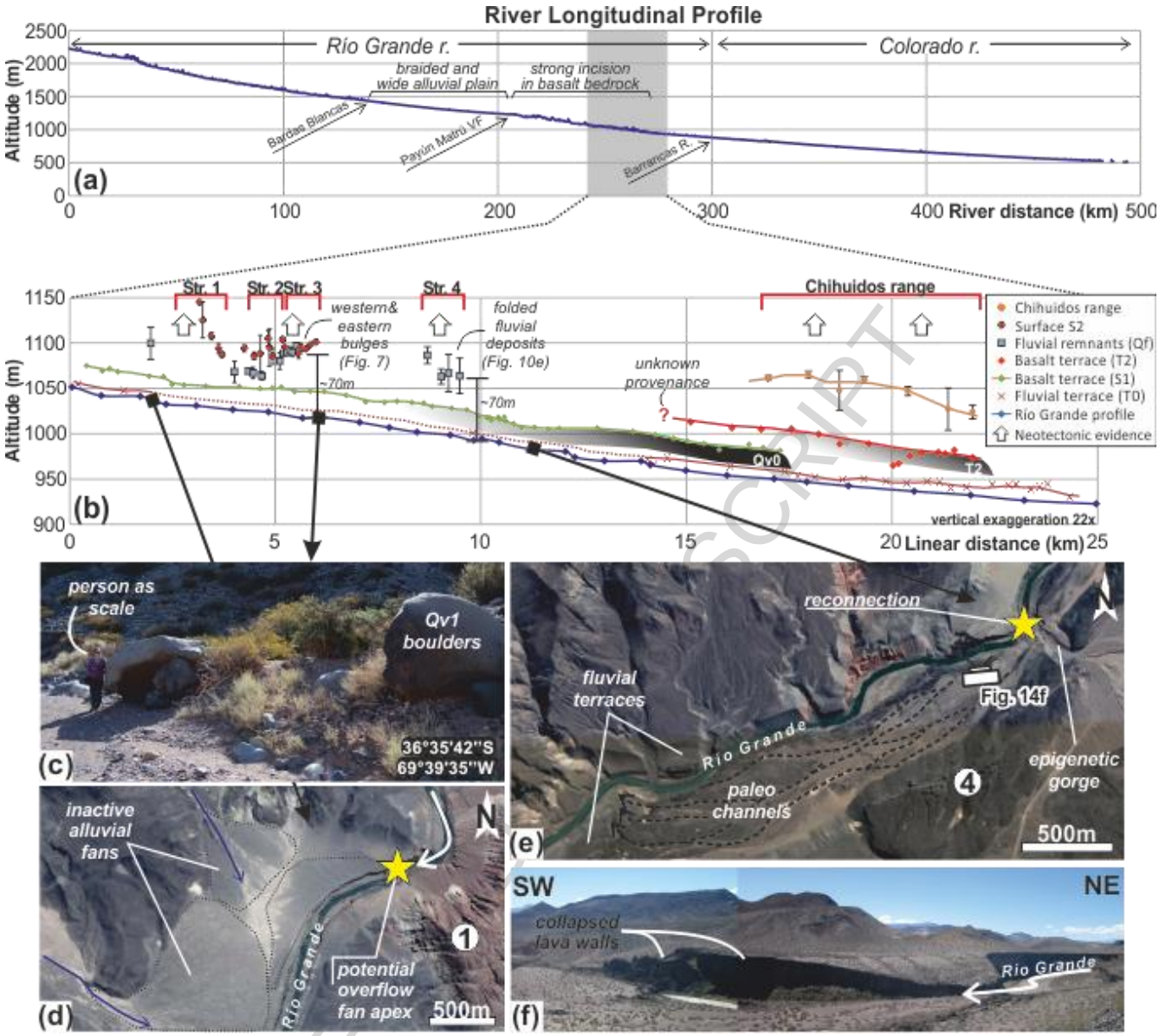

Figure 14. *Geomorphic elements in the study area along Rio Grande river. (a) Río Grande longitudinal profile from the Andes to the Colorado river in the foreland (see Figure 1 for location). Changes in behavior are noted. Shadowed area corresponds to the study area. (b) Transverse profile along line in Figure 6a. The altitude (obtained from SRTM data) of the different analyzed geomorphic elements is plotted. Also the spots where Quaternary uplift was interpreted are indicated. (c) Example of the chaotic deposit downstream the lacustrine deposits in Structure 3. Location in map is shown in Figure 7a. (d) Detailed of the alluvial processes on top of Qv0, associated with a temporary base level after the blockage of Río Grande river. (e) Detail of the downstream area of Qv0 where reconnection*

following damming is interpreted. (f) Field photograph showing collapse lava walls associated with dam removal. All numbers in white circles correspond to the western anticlines.

From a more regional perspective, in the Diamante river to the north (Fig. 1), Baker et al. (2009) have proposed that there is a close relation between major climate cycles and the aggradation stages they observed. Although in the Río Grande valley at least four Pleistocene glaciations are recognized in the upper basin (Espizua, 2004), at present there is no available data along the Andean foothills to correlate these climate cycles to any fluvial aggradation stage. Moreover, based on the field observations the fluvial terraces in the study region are comparatively much less developed than in the fluvial systems towards the north and potentially related to the loss of the river equilibrium profile related to the volcanic dams. Incision episodes in the Diamante river were also associated with the Quaternary uplift along the piedmont region (Baker et al. 2009). However, the scale of the Quaternary deformation presented in this work (of hundreds of meters), while interesting from a neotectonic perspective, may have not been enough to produce the observed changes in fluvial dynamics (in the scale of kilometers). Thus, the effects of both glacial/interglacial cycles and uplift history in the fluvial dynamics of the Río Grande river might have been obscured by the effects of the intense Pleistocene volcanism of the Payenia volcanic province.

5.2 Drainage network and landscape response to deformation

As stated by Costa et al. (2006a) for extra-andean regions of South America, with low deformation rates (<0.1 mm/yr), neotectonic structures usually do not reach to impose over the exogenous processes and, thus, do not achieve to modify the landscape significantly. In our case, despite the low uplift rates estimated for the analyzed structures (<0.8 mm/yr) we observed that the surface expression of neotectonic structures is not entirely absent. However, unless a good geological background is present, the information obtained from topography may be erratic. Given the absence of a clear fault scarp

related to the western anticlines that could serve to quantify neotectonic deformation in Cara Cura and Chihuidos ranges, uplift and slip rates had to be calculated with a considerable amount of uncertainty using basalt topography. More erodible material as fluvial terrace remnants or lacustrine deposits may be alternative deformation markers if more knowledge of the morphoclimatic conditions would be available (e.g. erosion/deposition rates).

Considering this limitation, a primary morphometric analysis was performed to check whether longitudinal stream profiles in this geomorphic environment were sensitive enough to record deformation. We showed that Cara Cura streams develop important knickzones in the mountain front associated with the resistant Triassic bedrock but not necessarily with any neotectonic activity. The higher drainage area of sub-basins I and III with respect to sub-basin II, would imply a higher stream power and therefore higher erosive capacity. This could explain why knickpoints and convex segments related to neotectonic structures were found only in sub-basin II (Fig. 11). Furthermore, in the Cara Cura western piedmont, the steepness index values were not much useful showing an expected variability, increasing downstream. Chihuidos region showed a similar situation. Knickpoints, in some cases, responded to the presence of volcanic dykes (streams III and IV; Fig. 12b) and in other cases, were related to the main fault scarp (Fig. 12). However, the fault scarp also coincides with the Cretaceous continental rocks outcrops which are more resistant than the Neogene deposits; thus, knickpoints from the main fault scarp, strictly, should not be taken into account as deformation markers. Meanwhile, concavity values in streams I and II (Fig. 12b) along the Chihuidos structure presented negative values which may be related to the emplacement of volcanic rocks at the outlet of the channels.

As Holbrook and Schumm (1999) suggest, longitudinal stream profiles may demonstrate the lack of adjustment of the channel to a new slope caused by tectonic perturbation only if alternative conditioning is discarded. As derived from the geomorphic evolution proposal (Section 5.1), Quaternary volcanism plays an important role controlling landscape dynamics, producing temporarily

dams (and the subsequent base level changes), relief inversion and lithological changes. After all of these considerations, in this type of complex geomorphic scenario, we conclude that longitudinal stream profiles should not be used as a standalone proxy of recent deformation.

5.3 Implications for regional context

Quaternary evolution of the study area is partly modulated by the onset of Payenia volcanic province, which was related both to a slab steepening followed by an extensional regime since 4 Ma (Ramos and Kay, 2006) or to an astenospheric anomaly impacting the lower crust (Burd et al., 2014). But, as it was described in Section 2.1, this transitional segment from shallow to normal subduction in the Andes shows, though fragmented, several neotectonic evidences which confirm that compressional tectonics dominated this region during the Quaternary (Fig. 1; Sections 1, 2.1).

In this work, neotectonic evidence was presented for the Cara Cura and Chihuidos ranges in the southern Malargüe FTB. Short wavelength anticlines (<2 km) affecting Quaternary units have been described, together with an 8 km-length fault scarp and drainage anomalies. This new evidence fills a gap of neotectonic information and reinforces the idea of Quaternary contraction at these latitudes. Yet, it is still a challenge to delineate a continuous Quaternary orogenic front along the Malargüe and Agrio FTBs eastern limit (Fig. 1) in part due to the high volumes of young volcanism in the region. But, also, the morphological signature of recent faults and folds studied in this area may be strongly conditioned by the low Quaternary deformation rates found. Despite the high uncertainties involved in the slip rates calculation for the Cara Cura region, which oscillate between 0.06 and 0.8 mm/yr, these values are as a general approximation one order of magnitude lesser than those from the San Rafael block, which range between 2.3 ± 1 mm/yr (Branellec et al., 2016a). The Quaternary slip rates and morphological signature in Cara Cura and Chihuidos ranges are more similar to those obtained in the Dorso de los Chihuidos anticline or even further south in the North Patagonian Andes (~40º S), where slip rates are in the order of 0.09 ± 0.025 mm/yr (Huyghe et al., 2015).

Furthermore, the evidence presented indicates that part of the Quaternary deformation was coetaneous with an intense volcanic activity from Los Callos and El Jinete effusive centers (Fig. 3). There are regional examples of the existent link between volcanism and compressional Quaternary tectonics in Tromen volcano, as demonstrated by Galland et al. (2007). These authors proposed different hypotheses to address this relationship, one of which suggests that a small magmatic body acted as a detachment level for the observed faults (Galland et al., 2007). In Cara Cura region several dykes and sills have been described (Guzmán et al., 2011), but yet there is not enough subsurface evidence to propose this connection neither in western Cara Cura piedmont nor in the Chihuidos range.

Another possible explanation for this neotectonic occurrence could also be related to volcanism, but in this time, through mantle behavior. As shown in Figure 1, SWAP branch of the asthenospheric anomaly described by Burd et al. (2014) impacts along a N-S elongated region that includes Tromen volcano, Reyes, Chihuidos and Cara Cura ranges, Payún Matrú VF and Palauco range (Burd et al., 2014). To the east, regional scale surface deformation related to the DEEP branch of the asthenospheric anomaly was presented by Astort et al. (2019), who posed that major river diversions and topographic swelling (with 50 – 70 km wavelength) in Auca Mahuida VF area, together with strong volcanism, are surficial effects of the mantle plume (e.g. Cox, 1989; Molin et al., 2004; Wegmann et al., 2007). Morphostructural evidence presented in this work does not adjust to that kind of deformation pattern. Nevertheless, Sagripanti et al. (2015) have related neotectonic occurrence in Tromen volcano (thrust faults and short wavelength anticlines, <5 km), to a crustal weakening caused by thermal perturbation of the SWAP branch of the described asthenospheric anomaly. Then, following those hypotheses, we can speculate about the existence of a possible link between the thermal anomalies and a long wavelength surface deformation pattern (> 50 km); meanwhile minor structures, such as those presented in this work, may result from local compressional stresses enhanced by, and not directly responsible of, the anomalous crustal thermal state. The asthenospheric anomaly conditioning effect

together with the low deformation rates found in the area can, then, account for the difficulties in delineating a continuous Quaternary orogenic front at these latitudes.

6. Conclusions

Field reconnaissance through the Río Grande valley in southern Mendoza Province revealed Quaternary units associated with a piedmont zone evolution affected by Quaternary folding and thrusting. A radiometric constraint indicates a 260 ± 70 ka age for a deformed lava flow. This contribution fills a gap of nearly 300 km of not previously recognized neotectonic activity in the Southern Central Andes. The evidences found show that tectonic activity in the Malargüe FTB front took place during the Quaternary. In particular over Cara Cura range, reverse faults affecting fluvial and lacustrine deposits, fault-related fold and groundshake related structures indicate neotectonic activity along west-vergent neotectonic anticlines. Also, different lava flows produced recurrent damming at the Río Grande river in the last 300 ka. Geomorphological evidence collected from the Cara Cura and Chihuidos ranges point to a complex history with volcanic and fluvial processes modeling the landscape and neotectonic activity being secondary but active in surface deformation. On the other hand, longitudinal channel profiles and concavity and steepness index calculations were performed in order to differentiate those morphometric signals produced by passive controls from those regarding tectonic deformation. Considering the ephemeral character of the tributaries and the erosion/deposition processes, the neotectonic signal obtained from the morphometric indicators was found to be weak, although some of the observed knickpoints and convex-up channel sections are related spatially to faults location.

Overall, the field observations and the morphometric results indicate that the mountain front at these latitudes absorbed contractional stresses during the Quaternary. A thermal weakening of the crust induced by the aforementioned asthenospheric anomaly, and related to the extended Quaternary

volcanic activity in the region, may have favored fault re-activation during the Pleistocene. Future studies may provide further data regarding the magnitude and persistence of this deformation.

Acknowledgments

This work was supported by the National Council of Science of Argentina and funded by PIP 2015-2017 (11220150100426CO). We thank SERNAGEOMIN (*Servicio Nacional Geológico y Minero de Chile*) for dating the lava sample. We acknowledge Diego Winocur for sharing discussions that improved this work, especially on volcanic evolution. Same for Eduardo Llambías, now may he rest in peace. This is the contribution RXX of the *Instituto de Estudios Andinos Don Pablo Groeber* (UBA-CONICET).

References

Astort, A., Colavitto, B., Sagripanti, L., García, H., Echaurren, A., Soler, S., Ruiz, F., Folguera, A., 2019. Crustal and mantle structure beneath the southern Patenia Volcanic Province using gravity and magnetic data. Tectonics 38, 144–158. https://doi.org/10.1029/2017TC004806

Álvarez Cerimedo, J., Orts, D., Rojas Vera, E., Folguera, A., Bottesi, G., Ramos, V.A., 2013. Mecanismos y fases de construcción orogénicos del frente oriental andino (36º S, Argentina). Andean Geol. 40, 504–520. https://doi.org/10.5027/andgeoV40n3-a06

Backé, G., Hervouët, Y., Dhont, D., 2006. Cenozoic extension vs. compression in the central Neuquén basin (37º–36º S, Argentina). In: Backbone of the Americas Patagonia to Alaska. Geol. Soc. Am., Abstract with programs, Special meeting, p. 111.

Baker, S.E., Gosse, J.C., McDonald, E.V., Evenson, E.B., Martínez, O., 2009. Quaternary history of the piedmont reach of Río Diamante, Argentina. J. S. Am. Earth Sci. 28, 54–73. https://doi.org/10.1016/j.jsames.2009.01.001

Bastías, H., Tello, G., Perucca, L., Paredes, J., 1993. Peligro sísmico y neotectónica. In: Ramos, V. (Ed.), Geología y Recursos Naturales de Mendoza. XII Congreso Geológico Argentino, II Congreso de Exploración de Hidrocarburos. Mendoza, pp. 645–658.

Bohm, M., Lüth, S., Echtler, H., Asch, G., Bataille, K., Bruhn, C., Rietbrock, A., Wigger, P. 2002. The Southern Andes between 36º and 40º S latitude: seismicity and average seismic velocities. Tectonophysics 356, 275–289. https://doi.org/10.1016/S0040-1951(02)00399-2

Branellec, M., Nivière, B., Callot, J.P., Regard, V., Ringenbach, J.C., 2016a. Evidence of active shortening along the eastern border of the San Rafael basement block: characterization of the seismic source of the Villa Atuel earthquake (1929), Mendoza province, Argentina. Geol. Mag. 153, 911–925. https://doi.org/10.1017/S0016756816000194

Branellec, M., Nivière, B., Callot, J.P., Ringenbach, J.C. and Ballard, J.F, 2016b. Mechanisms of basin contraction and reactivation in the basement involved Malargue fold-and thrust-belt, Central Andes (34°S-36°S). Geol. Mag. 153, 926–944. https://doi.org/10.1017/S0016756816000315

Burbank, D.W., Anderson, R.S., 2011. Tectonic geomorphology. John Wiley & Sons.

Burd, A.I., Booker, J.R., Mackie, R., Favetto, A., Pomposiello, M.C., 2014. Three-dimensional electrical conductivity in the mantle beneath the Payún Matrú Volcanic Field in the Andean backarc of Argentina near 36.5º S: Evidence for decapitation of a mantle plume by resurgent upper mantle shear during slab steepening. Geophys. J. Int. 198, 812–827. https://doi.org/10.1093/gji/ggu145

Casa, A., Yamin, M., Wright, E., Costa, C., Coppolecchia, M., Cegarra, M., Hongn, F., 2014. Deformaciones Cuaternarias de la República Argentina, Sistema de Información Geográfica. Instituto de Geología y Recursos Minerales, Servicio Geológico Minero Argentino. Buenos Aires, Argentina.

Cisneros, H., Ormeño, P., Bastías, H., 1989. Fallas cuaternarias en el sur mendocino y su posible relación con el sismo de 1929. 1º Reunión de Fallas Activas del NOA 1, San Juan, Argentina. pp. 58–62.

Cisneros, H., Bastias, H., 1993. Neotectónica del Borde oriental del Bloque de San Rafael. In: Ramos, V. (Ed.), Geología y Recursos Naturales de Mendoza. XII Congreso Geológico Argentino, II Congreso de Exploración de Hidrocarburos. Mendoza, pp. 3270–3276.

Chen, Y.W., Shyu, J.B.H., Chang, C.P., 2015. Neotectonic characteristics along the eastern flank of the Central Range in the active Taiwan orogen inferred from fluvial channel morphology. Tectonics 34, 2249–2270. https://doi.org/10.1002/2014TC003795

Cobbold, P.R., Rossello, E.A., 2003. Aptian to recent compressional deformation, foothills of the Neuquén Basin, Argentina. Mar. Pet. Geol. 20, 429–443. https://doi.org/10.1016/S0264-8172(03)00077-1

Costa C., Machette, M.N., Dart, R.L., Bastías, H.E., Paredes, J.D., Perucca, L.P., Tello, G.E., Haller, K.M., 2000. Map and Database of Quaternary Faults and Folds in Argentina, US Geological Survey Open-File Report 108, p. 75.

Costa, C., Audemard, F., Bezerra, F. H. R., Lavenu, A., Machette, M. N., París, G., 2006a. An overview of the main Quaternary deformation of South America. Rev. Asoc. Geol. Argent. 61, 461–479.

Costa, C., Cisneros, H., Salvarredi, J., Gallucci, A., 2006b. La neotectónica del margen oriental del bloque de San Rafael: Nuevas consideraciones. Asociación Geológica Argentina, Serie D: Publicación Especial 6, 33–40.

Cox, K.G., 1989. The role of mantle plumes in the development of continental drainage patterns. Nature 342, 873–877. https://doi.org/10.1038/342873a0

Cristallini, E., Tomezzoli, R., Pando, G., Gazzera, C., Martinez, J.M., Quiroga, J., Buhler, M., Bechis, F., Barredo, S., Zambrano, O., 2009. Controles precuyanos en la estructura de la Cuenca Neuquina. Rev. Asoc. Geol. Argent. 65, 248–264.

Dyhr, C.T., Holm, P.M., Llambías, E.J., 2013. Geochemical constraints on the relationship between the Miocene–Pliocene volcanism and tectonics in the Palaoco and Fortunoso volcanic fields, Mendoza Region, Argentina: New insights from $^{40}Ar/^{39}Ar$ dating, Sr–Nd–Pb isotopes and trace elements. J. Volcanol. Geoth. Res. 266, 50–68. https://doi.org/10.1016/j.jvolgeores.2013.08.005

Espizua, L.E., 2004. Pleistocene glaciations in the Mendoza Andes, Argentina. Developments in Quaternary Sciences 2 (III), 69–73. https://doi.org/10.1016/S1571-0866(04)80112-X

Fennell, L.M., Folguera, A., Naipauer, M., Gianni, G., Rojas Vera, E.A., Bottesi, G., Ramos, V.A., 2017. Cretaceous deformation of the southern Central Andes: synorogenic growth strata in the Neuquén Group (35º30'–37º S). Basin Res. 29, 51–72. https://doi.org/10.1111/bre.12135

Folguera, A., Ramos, V.A., Hermanns, R.L., Naranjo, J., 2004. Neotectonics in the foothills of the southernmost central Andes (37º–38º S): Evidence of strike-slip displacement along the Antiñir – Copahue fault zone. Tectonics 23, TC5008. https://doi.org/10.1029/2003TC001533

Folguera, A., Gianni, G., Sagripanti, L., Vera, E.R., Novara, I., Colavitto, B., Alvarez, O., Orts, D., Tobal, J., Introcaso, A., 2015. A review about the mechanisms associated with active deformation, regional uplift and subsidence in southern South America. J. S. Am. Earth Sci. 64, 511–529. https://doi.org/10.1016/j.jsames.2015.07.007

Galland, O., Hallot, E., Cobbold, P.R., Ruffet, G., de Bremond D'Ars, J., 2007. Volcanism in a compressional Andean setting: A structural and geochronological study of Tromen volcano (Neuquén province, Argentina). Tectonics 26, TC4010. https://doi.org/10.1029/2006TC002011

Germa, A., Quidelleur, X., Gillot, P.Y., Tchilinguirian, P., 2010. Volcanic evolution of the back-arc Pleistocene Payun Matru volcanic field (Argentina). J. S. Am. Earth Sci. 29, 717–730. https://doi.org/10.1016/j.jsames.2010.01.002

Giambiagi, L., Bechis, F., García, V., Clark, A.H., 2008. Temporal and spatial relationships of thick- and thin-skinned deformation: A case study from the Malargüe fold-and-thrust belt, southern Central Andes. Tectonophysics 459, 123–139. https://doi.org/10.1016/j.tecto.2007.11.069

Giambiagi, L., Ghiglione, M., Cristallini, E., Bottesi, G., 2009. Características estructurales del sector sur de la faja plegada y corrida de Malargüe (35º–36º S): distribución del acortamiento e influencia de estructuras previas. Rev. Asoc. Geol. Argent. 65, 140–153.

Guzmán, C.G., Cristallini, E.O., García, V.H., Bechis, F., 2011. Evolución del campo de esfuerzos horizontal desde el eoceno a la actualidad en la cuenca neuquina. Rev. Asoc. Geol. Argent. 68, 542–554.

Groeber, P., 1933. Descripción de la Hoja 31c “Confluencia de los ríos Grande y Barrancas”. Boletín de la Dirección de Minas y Geología, Buenos Aires, Argentina. pp. 38–72.

Holbrook, J., Schumm, S.A. 1999. Geomorphic and sedimentary response of rivers to tectonic deformation: a brief review and critique of a tool for recognizing subtle epeirogenic deformation in modern and ancient settings. Tectonophysics 305, 287–306. https://doi.org/10.1016/S0040-1951(99)00011-6

Huyghe, D., Nivière, B., Bonnel, C., 2015. Geomorphologic evidence for Plio-Quaternary shortening in the southern Neuquén basin (40º S, Argentina). Terra Nova 27, 426–432. https://doi.org/10.1111/ter.12176

Jordan, T.E., Burns, W.M., Veiga, R., Pángaro, F., Copeland, P., Kelley, S., Mpodozis, C., 2001. Extension and basin formation in the southern Andes caused by increased convergence rate: A mid-Cenozoic trigger for the Andes. Tectonics 20, 308–324. https://doi.org/10.1029/1999TC001181

Kay, S.M., Burns, W.M., Copeland, P., Mancilla, O., 2006. Upper Cretaceous to Holocene magmatism and evidence for transient Miocene shallowing of the Andean subduction zone under the northern Neuquén Basin. Geol. Soc. Am. Special Papers 407, 19–60.

Kirby, E., Whipple, K.X., 2001. Quantifying differential rock-uplift rates via stream profile analysis. Geology 29, 415–418. https://doi.org/10.1130/0091-7613(2001)029<0415:QDRURV>2.0.CO;2

Kirby, E., Whipple, K.X., 2012. Expression of active tectonics in erosional landscapes. J. Struct. Geol. 44, 54–75. https://doi.org/10.1016/j.jsg.2012.07.009

Kozlowski, E., Manceda, R., Ramos, V.A., 1993. Estructura. In: Ramos, V.A. (Ed.), Geología y Recursos Naturales de Mendoza. XII Congreso Geológico Argentino, II Congreso de Exploración de Hidrocarburos. Mendoza, pp. 235–256.

Legarreta, L., Gulisano, C., 1989. Análisis estratigráfico secuencial de la Cuenca Neuquina (Triásico superior-Terciario inferior). In: Chebli, G., Spaletti, L. (Eds.), Cuencas Sedimentarias Argentinas. Correlaciones Geológicas, Serie 6, 221–224.

Lupari, M.N., Spagnotto, S.L., Nacif, S.V., Yacante, G., García, H.P.A., Lince-Klinger, F., Sánchez, M.A., Triep, E., 2015. Sismicidad localizada en la zona del Bloque San Rafael, Argentina. Rev. Mex. Cienc. Geol. 32, 190–202.

Lupari, M., García, H.P.A., Nacif, S., Colavitto, B., Ruiz, F., 2016. Evidencia sismológica de actividad neotectónica en la sierra de Palauco y alrededores. Primer Simposio de Tectónica Sudamericana. Actas p. 91.

Manceda, R., Figueroa, D., 1995. Inversion of the Mesozoic Neuquén rift in the Malargüe fold and thrust belt, Mendoza, Argentina. In: Tankard, A.J., Suarez Soruco, R., Welsink, H.J. (Eds.), Petroleum Basins of South America. American Association of Petroleum Geologists, Memoir 42.

Marchetti, D.W., Cerling, T.E., Evenson, E.B., Gosse, J.C., Martínez, O., 2006. Cosmogenic exposures ages of lava flows that temporarily dammed the Río Grande and Río Salado, Mendoza Province, Argentina. In: Backbone of the Americas, Patagonia to Alaska. Asociación Geológica Argentina D, 9, 66.

Marchetti, D.W., Hynek, S.A., Cerling, T.E., 2014. Cosmogenic ^{3}He exposure ages of basalt flows in the northwestern Payún Matru volcanic field, Mendoza Province, Argentina. Quat. Geochronol. 19, 67–75. https://doi.org/10.1016/j.quageo.2012.10.004

Mescua, J.F., Giambiagi, L.B., Ramos, V.A., 2013. Late Cretaceous uplift in the Malargüe fold-and-thrust belt (35º S), southern Central Andes of Argentina and Chile. Andean Geol. 40, 102–116. https://doi.org/10.5027/andgeoV40n1-a05

Messager, G., Nivière, B., Martinod, J., Lacan, P., Xavier, J.P. 2010. Geomorphic evidence for Plio-Quaternary compression in the Andean foothills of the southern Neuquén Basin, Argentina. Tectonics 29, TC4003. https://doi.org/10.1029/2009tc002609

Messager, G., Nivière, B., Lacan, P., Hervouët, Y., Xavier, J.P., 2014. Plio-Quaternary thin-skinned tectonics along the crustal front flexure of the southern Central Andes: a record of the regional

stress regime or of local tectonic-driven gravitational processes? Int. J. Earth Sci. 103, 929–951. https://doi.org/10.1007/s00531-013-0983-4

Molin, P., Pazzaglia, F.J., Dramis, F., 2004. Geomorphic expression of active tectonics in a rapidly-deforming forearc, Sila Massif, Calabria, southern Italy. Am. J. Sci. 304, 559–589. https://doi.org/10.2475/ajs.304.7.559

Narciso, V., Santamarina, G., Zanettini, J.C., 2000. Hoja Geológica 3769-I "Barrancas" (1:250000). SEGEMAR, Boletín 253. Buenos Aires, Argentina.

Nullo, F.E., Stephens, G., Combina, A., Dimieri, L., Baldauf, P., Bouza, P., Zanettini, J.C., 2005. Hoja Geológica 3569-III "Malargüe" (1:250000). SEGEMAR, Boletín 346. Buenos Aires, Argentina.

Orts, D.L., Folguera, A., Giménez, M., Ramos, V.A., 2012. Variable structural controls through time in the Southern Central Andes (~36º S). Andean Geol. 39, 220–241. http://dx.doi.org/10.5027/andgeoV39n2-a02

Polanski, J., 1954. Rasgos geomorfológicos del territorio de la provincia de Mendoza. Ministerio Economía, Instituto Investigaciones económicas y tecnológicas, Cuadernos de investigaciones y estudios, 4. Ministerio de Economía del Gobierno de Mendoza, Mendoza, pp. 4–10.

Ramos, V.A., 2000. The Southern Central Andes. In: Cordani, U.G., Milani, E.J., Thomaz Filho, A., Campos, D.A. (Eds.), Tectonic Evolution of South America. 31º International Geological Congress, Río de Janeiro, pp. 560–604.

Ramos, V.A., Folguera, A., 2005. Tectonic evolution of the Andes of Neuquén: constraints derived from the magmatic arc and foreland deformation. Geological Society London, Special Publications 252, 15–35.

Ramos, V.A., Folguera, A., 2011. Payenia volcanic province in the Southern Andes: An appraisal of an exceptional Quaternary tectonic setting. J. Volcanol. Geoth. Res. 201, 53–64. https://doi.org/10.1016/j.jvolgeores.2010.09.008

Ramos, V.A., Kay, S.M., 2006. Overview of the tectonic evolution of the southern Central Andes of Mendoza and Neuquén (35º–39º S latitude). Geol. Soc. Am. Spec. Pap. 407, 1–17.

Ramos, V.A., Litvak, V.D., Folguera, A., Spagnuolo, M., 2014. An Andean tectonic cycle: from crustal thickening to extension in a thin crust (34º–37º SL). Geosci. Front. 5, 351–367. https://doi.org/10.1016/j.gsf.2013.12.009

Sagripanti, L., Bottesi, G., Naipauer, M., Folguera, A., Ramos, V.A., 2011. U/Pb ages on detrital zircons in the southern central Andes Neogene foreland (36º–37º S): Constraints on Andean exhumation. J. S. Am. Earth Sci. 32, 555–566. https://doi.org/10.1016/j.jsames.2011.03.010

Sagripanti, L., Vera, E.A.R., Gianni, G.M., Folguera, A., Harvey, J.E., Farías, M., Ramos, V.A., 2015. Neotectonic reactivation of the western section of the Malargüe fold and thrust belt (Tromen volcanic plateau, Southern Central Andes). Geomorphology 232, 164–181. https://doi.org/10.1016/j.geomorph.2014.12.022

Sagripanti, L., Folguera, A., Fennell, L., Vera, E.A.R., Ramos, V.A., 2016. Progression of the deformation in the Southern Central Andes (37º S). In: Folguera, A., Naipauer, M., Sagripanti, L., Ghiglione, M., Orts, D., Giambiagi, L. (Eds.), Growth of the Southern Andes. Springer Earth System Sciences. Springer, Cham. pp. 115–132. https://doi.org/10.1007/978-3-319-23060-3_6

Sagripanti, L., Colavitto, B., Jagoe, Lucía., Folguera, A., Costa, C., 2018. A review about the quaternary upper-plate deformation in the Southern Central Andes (36º–38° S): A plausible interaction between mantle dynamics and tectonics. J. S. Am. Earth Sci. 87, 221 - 231. https://doi.org/10.1016/j.jsames.2017.11.008

Schwanghart, W., Scherler, D., 2014. TopoToolbox 2–MATLAB-based software for topographic analysis and modeling in Earth surface sciences. Earth Surface Dynamics 2, 1–7.

Silvestro, J., Kraemer, P., Achilli, F., Brinkworth, W., 2005. Evolución de las cuencas sinorogénicas de la Cordillera Principal entre 35º–36º S, Malargüe. Rev. Asoc. Geol. Argent. 60, 627–643.

Silvestro, J., Atencio, M., 2009. La cuenca cenozoica del río Grande y Palauco: edad, evolución y control estructural, faja plegada de Malargüe. Rev. Asoc. Geol. Argent. 65, 154–169.

Spagnuolo, M.G., Litvak, V.D., Folguera, A., Bottesi, G., Ramos, V.A., 2012. Neogene magmatic expansion and mountain building processes in the southern Central Andes, 36º–37º S, Argentina. J. Geodyn. 53, 81–94. https://doi.org/10.1016/j.jog.2011.07.004

Stolar, D., Roe, G., Willett, S., 2007. Controls on the patterns of topography and erosion rate in a critical orogeny. J. Geophys. Res. 112, F04002. https://doi.org/10.1029/2006JF000713.

Stewart, I. S., Hancock, P.L., 1990. What is a fault scarp. Episodes 13, 256–263.

Tassara, A., Echaurren, A., 2012. Anatomy of the Andean subduction zone: three-dimensional density model upgraded and compared against global-scale models. Geophys. J. Int. 189, 161–168. https://doi.org/10.1111/j.1365-246X.2012.05397.x

Tunik, M., Folguera, A., Naipauer, M., Pimentel, M., Ramos, V.A., 2010. Early uplift and orogenic deformation in the Neuquén Basin: constraints on the Andean uplift from U–Pb and Hf isotopic data of detrital zircons. Tectonophysics 489, 258–273. https://doi.org/10.1016/j.tecto.2010.04.017

Turienzo, M., Dimieri, L., Frisicale, C., Araujo, V., Sánchez, N., 2012. Cenozoic structural evolution of the Argentinean Andes at 34º 40' S: A close relationship between thick and thin-skinned deformation. Andean Geol. 39, 317–357. http://dx.doi.org/10.5027/andgeoV39n2-a07

USGS. 2015. Shuttle Radar Topography Mission (SRTM) 1 Arc-Second Global. United States Geological Survey. https://doi.org/10.5066/F7PR7TFT

van Gorp, W., Veldkamp, A., Temme, A.J.A.M., Maddy, D., Demir, T., van der Schriek, T., Reimann, T., Wallinga, J., Wijbrans, J., Schoorl, J.M., 2013. Fluvial response to Holocene volcanic damming and breaching in the Gediz and Geren rivers, western Turkey. Geomorphology 201, 430–448. https://doi.org/10.1016/j.geomorph.2013.07.016

van Hinsbergen, D.J., 2011. Short note on the use of Neotectonic and Palaeotectonic Nomenclature. Turkish J. Earth Sci. 20, 161–165. https://doi.org/10.3906/yer-1002-15

Veldkamp, A., Schoorl, J.M., Wijbrans, J.R., Claessens, L., 2012. Mount Kenya volcanic activity and the Late Cenozoic landscape reorganisation in the upper Tana fluvial system. Geomorphology 145, 19–31. https://doi.org/10.1016/j.geomorph.2011.10.026

Wegmann, K.W., Zurek, B.D., Regalla, C.A., Bilardello, D., Wollenberg, J.L., Kopczynski, S.E., Ziemann, J.M., Haight, S.L., Apgar, J.D., Zhao, C., Pazzaglia, F.J., 2007. Position of the Snake River watershed divide as an indicator of geodynamic processes in the greater Yellowstone Region, western North America. Geosphere 3, 272–281. https://doi.org/10.1130/GES00083.1

Wobus, C.W., Whipple, K.X., Hodges, K.V., 2006. Neotectonics of the central Nepalese Himalaya: Constraints from geomorphology, detrital $^{40}Ar/^{39}Ar$ thermochronology, and thermal modeling. Tectonics 25, TC4011. https://doi.org/10.1029/2005TC001935

Zárate, M., Folguera, A., 2014. Planation surfaces of Central Western Argentina. In: Rabassa J., Ollier C. (Eds.) Gondwana Landscapes in southern South America. Springer Earth System Sciences. Springer, Dordrecht. pp. 365–392. https://doi.org/10.1007/978-94-007-7702-6_13

Fig1.eps; Size: 1.5 column

Figure 1. (a) Regional context of the Southern Central Andes and the location of Figure 1b; Chilean-Pampean Flat Subduction Zone and Southern Volcanic Zone are shown as well as subducted slab depth contours (Tassara and Echaurren, 2012). (b) Main morphostructural units in the study area in the southernmost Central Andes. Structures of interest are labeled in blue ellipses (P: Palauco; CC: Cara Cura; C: Chihuidos; R: Reyes; Y: Yesera; DCh: Dorso de los Chihuidos). White dashed rectangles show recent neotectonic studies in the region (references in white letters). Yellow and violet curves are, respectively, the 33 km and 55 km depth contours of the obtained 35 Ohm-m resistivity from a 3D inversion of a magnetotelluric survey depict an asthenospheric anomaly interpreted as a mantle plume at depth (Burd et al., 2014).

Fig2.eps; Size: Single column

Figure 2. (a) Geologic map of southern Malargüe fold and thrust belt front (modified from Narciso et al., 2004; Nullo et al., 2005). Q: Quaternary; T: Tertiary; K: Cretaceous; J: Jurassic; P-Tr: Permo-Triassic. Location shown in Figure 1.

Fig3.eps; Size: 2 columns

Figure 3. Geology of Cara Cura range. (a) Structure and main geological units exposed. Short wavelength anticlines to the west of Cara Cura range are numbered from 1 to 4. Geology and structure are modified from Fennell et al. (2017). Location shown in Figure 2a. (b) Structural cross-section A-B. In gross lines the two main west-vergent basement faults are highlighted. (c) Structural interpretation for northern tip of Structure 3. References are for both map and section. P: Permian; Tr: Triassic; J: Jurassic; K: Cretaceous; Q: Quaternary; c: continental rocks; l: lacustrine deposits; v: volcanic rocks.

Fig4.eps; Size: Single column

Figure 4. Geological observations of Chihuidos range. (a) Satellite image of Chihuidos monocline. Main drainage network can be observed as well as the main scarps (fault scarp and terrace risers), also included geological units. Location shown in Figure 2a. (b) Digital elevation model showing the position of Chihuidos range fault scarp (white arrows). (c) Reconstruction of Chihuidos monocline forelimb. (d) Backlimb of Chihuidos monocline with slightly tilted upper Miocene deposits. J-Km: Jurassic-Cretaceous marine rocks; Kc: Cretaceous continental rocks; Tc: Upper Miocene continental rocks; Qv0: Los Volcanes basalts; Qv: Quaternary volcanic rocks (undefined).

Fig5.eps; Size: 2 columns

Figure 5. Quaternary geology of Cara Cura range western slope. (a) Geologic map with main Quaternary units. The location of a $^{40}Ar/^{39}Ar$ age presented in this work is indicated with a yellow star. Numbers in white circles refer to western anticlines, Structures 1 – 4. Blue dashed line corresponds to the area with playa-lake deposit outcrops. (b) Stratigraphic column of Cara Cura and Chihuidos areas. Colors correspond to the geological units of Figure 5a. References for both figures are indicated. (c) Field photograph corresponding to Los Volcanes basalts (Qv0) affected by fluvial erosion at the northern tip of Structure 1.

Fig6.eps; Size: 2 columns

Figure 6. (a) Satellite image showing the distribution of fluvial terrace remnants (Qf), Los Volcanes basalts (Qv0), erosional surface S2 along the Río Grande valley at Cara Cura segment and terraces T0-T2 at Chihuidos segment. Location of topographic profiles A – D is indicated. Numbers in white circles refer to the western anticlines. White squares correspond to the other figures' location. (b) Surficial aspect of the fluvial terrace remnants. (c) Field photograph taken from the same location as Figure 6b. A ~20 m incision over Los Volcanes basalts (Qv0) can be seen. (d)Example of erosional surface S2 beveling Cretaceous rocks (Kc). A ~10m relief with respect to surface S1 is indicated. (e) Example of

erosional surface S2 beveling lacustrine deposits. A ~20 m relief with respect to surface S1 is indicated. (f) Topographic profiles A and B, transverse to Río Grande river at western Cara Cura piedmont, and C and D, transverse to Río Grande river at Chihuidos range; S1 and T2 correspond to different basalt terrace levels. T0 corresponds to the lowest fluvial terrace. Profile units are in meters in both axis. VE is vertical exaggeration. (See text for further details)

Fig7.eps; Size: 2 columns

Figure 7. Evidences of Quaternary faulting. (a) Satellite image showing western and eastern bulges (yellow contours), the structural interpretation for this area and the location of P1-P5 topographic profiles. Location shown in Figure 5a. Kc: Cretaceous continental rocks; Qv1: Los Callos basalts. Number in white circle indicates Structure 3. Black square corresponds to the location of Figure 7c. (b) Topographic profiles P1-P5. Structures are interpreted from topography, except documented faults in profile P4. References for line colors are included. VE is vertical exaggeration. (c) Field picture showing a set of reverse faults affecting Quaternary strata. The west vergent fault plane is interpreted from the relationship between fluvial conglomerates and fine sand deposits (see text for further details).

Fig8.eps; Size: 2 columns

Figure 8. (a) Playa-lake deposits scattered through Cara Cura western slope (in yellow). White circled numbers refer to the western anticlines. (b) Lacustrine strata tilted 18º to NNW, covered by alluvial deposits and a basalt flow. (c) Tilted lacustrine beds covered by gravels and alluvial deposits. (d) Field photo and interpretation of folded and faulted lacustrine benches covered by fluvial gravels. (e) Detailed photo of the vertical benches from the forelimb. Ql: lacustrine; Qv2: El Jinete basalts; Qa: alluvial; Qf: fluvial.

Fig9.eps; Size: 2 columns

Figure 9. Evidences of soft sediment deformation. (a) Playa-lake deposits scattered through Cara Cura western slope (in yellow). White circled numbers refer to the western anticlines. (b) Lacustrine sediments outcrop, with horizontal lamination at the bottom and top, and two levels (1 and 2) with convolute and chaotic stratification. (c) Detail picture from the contact between undeformed and deformed levels. (d) Lacustrine deposits outcrop showing internal deformation. (e) Intrasedimentary fault affecting slightly folded levels. (f) Convolute lamination, pencil as scale. (g) and (h) Convolute lamination in an outcrop at the south of structure 1 (location in Fig. 9a; GPS location is almost the same for both pictures).

Fig10.eps; Size: 1.5 columns

Figure 10. Detail of Structure 4. (a) Oblique Google Earth view of Structures 3 and 4. Los Callos basalts (yellow dashed line) spread over the piedmont, being affected by a blind west vergent thrust. White squares and camera drawings indicate other figures' location. (b) Longitudinal cracks at the anticline hinge of Structure 4 indicated by white arrows as a consequence of folding stresses. (c) Northern tip of Structure 4. Dashed line corresponds to the interpreted internal structure. (d) Frontal scarp of Structure 4. A watergap can be seen, coincident with the lateral contact between Los Callos basalts (Qv1) and fluvial terrace deposits (Qf). (e) Field photograph taken from the south of Structure 4 showing fluvial terrace deposits slightly folded. (f) Topographic profile as showed in Figure 10a. Shadowed area corresponds to the surface expression of Structure 4 over Los Callos basalts.

Fig11.eps; Size: 2 columns

Figure 11. Morphometry of Cara Cura range western rivers. (a) Digital elevation model with the three drainage sub-basins analyzed and location of knickpoints; white/black numbers refer to their height in meters. Geological structures are also plotted. (b) Longitudinal stream profiles of sub-basins I to III. Knickpoints or knickzones (shadowed) associated features are indicated. (c) Log-log slope vs. area

plots. Red square highlights a segment in river II with predominantly negative concavity values, coincident with the fault zone segment.

Fig12.eps; Size: 2 columns

Figure 12. (a) Satellite image of the Chihuidos range. Main drainage sub-basins are highlighted in white dashed lines. River network is shown together with the main scarps that limit the Chihuidos structure to the east. (b) Longitudinal river profiles of the four basins indicated in Figure 12a. Red concavity values indicate almost convex or convex segments. (c) Oblique Google Earth view of the range, where white arrows indicate the position of the two fault scarps and blue squares highlight river segments of higher sinuosity.

Fig13.eps; Size: 1.5 columns

Figure 13. Proposed schematic evolution of Río Grande river segment to the west of the Cara Cura range (see text for further details). Six stages are proposed (1 to 6), the last corresponding to present day conditions. Locations where Río Grande was blocked (black stars) and where dam removal was initiated (yellow stars) are indicated. White arrows in Stage 4 correspond to structures where Quaternary uplift was interpreted. Dashed area in captions a, b and d refer to the width of the paleo-Río Grande valley. Numbers in white circles in caption f correspond to the western anticlines (see text for further details).

Fig14.eps; Size: 2 columns

Figure 14. Geomorphic elements in the study area along Rio Grande river. (a) Río Grande longitudinal profile from the Andes to the Colorado river in the foreland (see Figure 1 for location). Changes in behavior are noted. Shadowed area corresponds to the study area. (b) Transverse profile along line in Figure 6a. The altitude (obtained from SRTM data) of the different analyzed geomorphic elements is

plotted. Also the spots where Quaternary uplift was interpreted are indicated. (c) Example of the chaotic deposit downstream the lacustrine deposits in Structure 3. Location in map is shown in Figure 7a. (d) Detailed of the alluvial processes on top of Qv0, associated with a temporary base level after the blockage of Río Grande river. (e) Detail of the downstream area of Qv0 where reconnection following damming is interpreted. (f) Field photograph showing collapse lava walls associated with dam removal. All numbers in white circles correspond to the western anticlines.

Highlights

- New evidence of neotectonic activity in the Southern Central Andes (36º-37ºS)
- Anomalies in longitudinal river profiles can be related to Quaternary structures
- Reverse faults and folds support a middle to late Pleistocene compressional regime
- Volcanic – fluvial interplay is here a major control on landscape evolution
- A correlation exists between recent deformation and asthenospheric anomalies